Ca' Foscari
University
of Venice

Master's Degree programme
in Data Analytics for Business and Society

Final Thesis

Impact of Climate Change on Rainfall Distribution

Analyzing the shift towards More Extreme
Short-Duration Events over Longer ones

Supervisor
Ch. Prof. Ilaria Prosdocimi

Graduand
Alessandro Marinozzi
Matriculation Number 889988

Academic Year
2023 / 2024

TABLE OF CONTENTS

ABSTRACT

Climate change represents one of the most significant challenges of our time, influencing global climate patterns and impacting ecosystems, sea levels, and weather events. This thesis explores the impact that the climate change has on the distribution of rainfall, with a particular focus on the increasing frequency and intensity of short-duration rainfall events compared to longer-duration ones. This phenomenon has substantial implications in terms of socio-economic costs.

This study is conducted on the dataset furnished by the Autonomous Province of Trentino, which collects rainfall observations at five-minute intervals. This high-resolution data offers opportunity to analyze rainfall patterns in detail, enabling a comprehensive assessment of the hypothesis that short-duration rainfall events are increasing at a faster rate than longer-duration events.

Through detailed statistical analysis and comparison with literature about the topic, this dissertation aims to provide new insights into the dynamics of rainfall distribution under changing climate conditions. The findings are expected to enhance understanding of the implications of these changes and inform future climate adaptation and mitigation strategies, in order to tackle the increasing socio-economic costs associated with extreme precipitation events.

LIST OF FIGURES

1. INTRODUCTION

1.1 CLIMATE CHANGE PHENOMENA AND ITS COST

Defined as a significant and lasting alteration in global and regional climate patterns, Climate Change is principally attributed to anthropogenic activities, particularly the emission of greenhouse gases such as carbon dioxide (CO_2) and methane (CH_4). This phenomenon not only alters global average temperatures but also impacts various aspects of the Earth's systems, including ecosystems, sea levels, and weather patterns. The attention to climate change has grown exponentially in recent decades and the topic is of cardinal importance nowadays, as evidenced by the widespread media coverage, political discourse, and scientific research dedicated to understanding and mitigating its effects (IPCC, 2021; World Bank, 2024).

Reports from the Intergovernmental Panel on Climate Change emphasize that global warming is incontrovertible and that human activities are the main cause of this it (IPCC, 2021). The IPCC's Sixth Assessment Report of 2021 underscores the urgent need for action, highlighting how continued emissions will lead to increasingly severe and irreversible impacts on the environment and human societies.

International agreements, such as the Paris Agreement of 2015, plan to limit global temperature increases to well below 2°C above pre-industrial levels, reflecting a global consensus on the necessity of addressing this issue (European Commission, 2020). Despite these efforts, global greenhouse gas emissions continue to rise, signaling the need for more aggressive and coordinated actions to combat climate change (Deloitte, 2022).

The economic costs associated with climate change are massive and multifaceted, impacting various sectors and regions globally. A recent report by the Deloitte Economics Institute alerts that inaction on climate change could cost the global economy $178 trillion by 2070, matching to a 7.6% reduction in global GDP for that year alone (Deloitte, 2022; Deloitte United States, 2023).

The World Bank underscores that climate change could lead approximately 132 million people into extreme poverty by 2030. The global cost of extreme weather events linked to climate change could exceed $520 billion annually (World Bank, 2024).

These figures illustrate the profound economic implications of climate change and the necessity for robust adaptation and mitigation measures.

Moreover, the financial burden of climate change is not evenly distributed, often disproportionately affecting the most vulnerable populations. Developing countries, which contribute the least to global emissions, are frequently the hardest hit by the adverse effects of climate change (IPCC, 2021; World Bank, 2024).

Economic costs include the destruction of infrastructure, loss of biodiversity, increased healthcare expenses due to climate-related illnesses, and strong impacts on food and water security. For example, agricultural sectors worldwide face decreased crop yields and increased volatility in food supply due to changing precipitation patterns and more frequent extreme weather events. This not only threatens food security but also leads to higher food prices and economic instability (Deloitte, 2022; World Bank, 2024).

The health sector also bears significant economic damages. Climate change contributes to the spread of vector-borne diseases and worsen respiratory and cardiovascular aspects due to higher levels of air pollution. These health impacts result in increased healthcare costs, lost labor productivity, and reduced quality of life. According to the World Health Organization, the direct damage costs to health (excluding costs in health-determining sectors such as agriculture and water and sanitation) are estimated to be between $2-4 billion per year by 2030 (WHO, 2021).

In summary, the economic implications of climate change are far-reaching and necessitate urgent and sustained global action to diminish its effects. Addressing climate change requires comprehensive strategies that include huge investments in renewable energy, sustainable infrastructure, and resilient agricultural practices. Policymakers, businesses, and individuals must collaborate to reduce greenhouse gas emissions and build resilience against the unavoidable impacts of climate change, ensuring a sustainable future for all (European Commission, 2020; Deloitte, 2022).

Moving from a global perspective to a regional focus, Europe itself faces significant economic burdens due to climate change. According to the European Environment Agency, Europe has experienced substantial economic losses from weather and climate-related extremes. From 1980 to 2020, these losses amounted to between €450 billion and €520 billion, primarily due to extreme weather events such as floods, storms, and heatwaves (European Environment

Agency, 2023). These events have become more frequent and intense, exacerbating economic vulnerabilities across the continent.

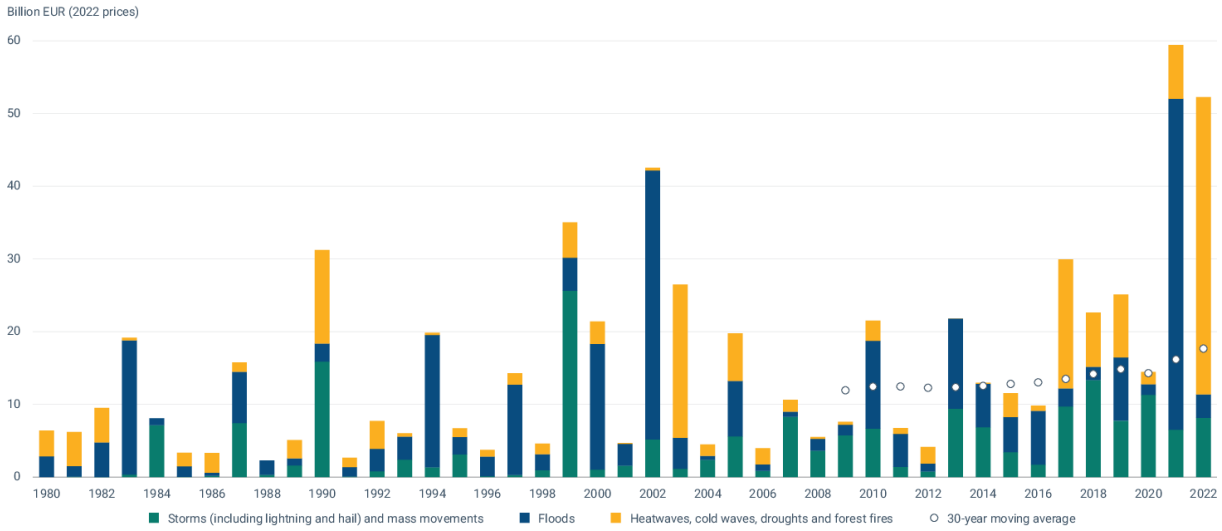

Figure 1.1: Trend of the economic cost of Climate Change for European Countries. (Retrieved from European Environment Agency)

In Southern Europe, countries like Italy are particularly vulnerable to the impacts of climate change due to their geographical and climatic characteristics. Italy is the third country in Europe terms for the economic loss suffered by the climate change in absolute terms, following Germany and France (Eurostat, 2022).

It faces a variety of climate-related challenges, including increased temperatures, rising sea levels, and more frequent and severe weather events such as floods, droughts, and heatwaves. These phenomena have significant economic implications for various sectors, particularly agriculture, tourism, and infrastructure. According to the European Environment Agency, between 1980 and 2020, climate-related losses in Italy ranged between €90 billion and €150 billion (European Environment Agency, 2023).

These losses underscore the urgent need to implement robust climate adaptation and mitigation strategies. Investing in climate-resilient infrastructure, promoting sustainable agricultural practices, and enhancing disaster preparedness are critical measures to reduce future economic losses and build resilience against climate change impacts. The European Union supports member states, including Italy, in their climate adaptation efforts through

various funding mechanisms and initiatives. The European Green Deal aims to make Europe the first climate-neutral continent by 2050, with significant investments directed towards sustainable infrastructure, renewable energy, and climate resilience projects (European Commission, 2020).

1.2 RELATIONSHIP BETWEEN CLIMATE CHANGE AND PRECIPITATION PATTERNS

In the intricate and ever-changing realm of contemporary climate dynamics, the alteration of precipitation patterns stands out as a critical and pivotal aspect of climate change. Over the past few decades, the Earth's climate system has experienced profound and significant modifications, leading to notable shifts in the distribution, intensity, and frequency of rainfall events across various regions (IPCC, 2021; Fischer & Knutti, 2016). These changes manifest as prolonged droughts in some areas and intensified rainfall or flooding in others (Zhang & Villarini, 2020).

Understanding the evolving relationship between climate change and precipitation patterns is essential for a multitude of reasons. It plays a crucial role in informing decision-making processes at both local and global levels, enabling policymakers to develop and implement effective adaptation strategies. Moreover, this understanding is vital for anticipating future climatic conditions and preparing for their potential impacts on ecosystems, agriculture, water resources, and human settlements (Marvel et al., 2019; Prein et al., 2017).

Central to the understanding of precipitation changes under a warming climate is the Clausius-Clapeyron relationship, which elucidates the fundamental connection between temperature and atmospheric moisture content. This thermodynamic principle describes how the capacity of the atmosphere to hold water vapor increases with temperature. Specifically, according to the Clausius-Clapeyron equation, for every degree Celsius rise in temperature, the atmosphere can hold approximately 7% more water vapor (Fischer & Knutti, 2016). Recent research has shown that for hourly and sub-hourly precipitations, this scaling can increase to approximately 14% per degree Celsius rise, known as the Super-Clausius–Clapeyron Scaling (Lenderink et al., 2017).

As global temperatures continue to increase due to the continuous emissions of greenhouse gases, the potential for enhanced atmospheric moisture content also rises. This sets the stage for profound alterations in precipitation patterns. Enhanced atmospheric moisture can lead to more intense and frequent rainfall events, contributing to phenomena such as increased heavy rainfall and flooding (IPCC, 2021). Conversely, the redistribution of moisture and changes in circulation patterns can also exacerbate drought conditions in some regions, creating a more volatile and unpredictable hydrological cycle (Marvel et al., 2019; Prein et al., 2017).

Climate change, propelled by anthropogenic activities and attendant changes in radiative forcing, has catalyzed a spectrum of atmospheric adjustments, profoundly reshaping precipitation regimes across the globe (Zhang & Villarini, 2020). Moreover, increased atmospheric moisture content can influence atmospheric stability and convection processes. Enhanced water vapor can lead to more vigorous convective activity, which is a key driver of thunderstorms and heavy rainfall events. The enhanced latent heat release during condensation processes further energizes the atmosphere, potentially increasing the severity of weather events (Fischer & Knutti, 2016).

To fully grasp the implications of the Clausius-Clapeyron relationship in the context of climate change, it is essential to integrate this understanding with observational data and climate models. These tools help quantify the impacts of increased atmospheric moisture on precipitation patterns and provide projections for future climate scenarios. They also assist in identifying regions particularly vulnerable to changes in precipitation, thereby informing adaptation and mitigation strategies (IPCC, 2021; Lenderink et al., 2017).

Contemporary research endeavors, informed by an amalgamation of observational evidence, advanced climate modeling, and interdisciplinary synthesis, provide compelling insights into the evolving nature of precipitation under a changing climate. Recent studies confirm the escalating trends in precipitation extremes, characterized by intensified rainfall events, prolonged droughts, and amplified hydrological variability (Marvel et al., 2019). Notably, the disproportionate increase in short-duration rainfall events relative to longer-duration events has emerged as a salient feature of contemporary precipitation patterns, accentuating concerns over water-related hazards and ecosystem resilience (Fischer & Knutti, 2016; Zhang & Villarini, 2020).

This phenomenon emphasizes the urgent need for proactive adaptation measures to mitigate the impacts of changing precipitation patterns on vulnerable communities and ecosystems.

1.3 SOCIO-ECONOMIC IMPACT OF RAINFALL EVENTS

Short-duration, high-intensity rainfall events, exacerbated by climate change, pose significant socio-economic challenges globally, impacting agriculture, urban infrastructure, and flood management systems. The intensification of these weather patterns necessitates urgent adaptive measures to mitigate their adverse effects (Taguchi et al., 2019; Yin et al., 2018).

Evidence from around the world confirms the tremendous cost of changing rainfall patterns. In sub-Saharan Africa, agriculture, a primary source of livelihood for many, faces severe disruptions due to erratic precipitations. Studies suggest that these sudden downpours can lead to soil erosion, loss of arable land, and decreased crop yields, exacerbating food insecurity and economic instability (Nkonya et al., 2016; World Bank, 2019). For instance, projections indicate that by 2050, maize yields in the region could decline by up to 20%, affecting millions of smallholder farmers (World Bank, 2019).

Urban areas worldwide face increasing risks from heavy rainstorms, particularly in cities with aging infrastructure and inadequate drainage systems. Research in cities like Houston, Texas, and Miami, Florida, highlights the escalating threat of urban flooding due to climate change-induced rainfall patterns. In Houston alone, the estimated annual cost of urban flooding exceeds $1.9 billion (Siddique et al., 2020). Furthermore, projections suggest that by 2100, the number of people at risk of coastal flooding in urban areas could increase by up to 300 million globally (Hinkel et al., 2014; Becker et al., 2018).

Island nations and coastal regions in Oceania are highly susceptible to the impacts of these phenomena, compounded by rising sea levels and storm surges. Studies in countries like Fiji, Samoa, and the Cook Islands underscore the intertwined nature of extreme rainfall and coastal inundation, threatening critical infrastructure, livelihoods, and cultural heritage. For instance, in the Pacific Island region, it is estimated that the annual damage from coastal flooding could reach $1.4 billion by 2100 (Nurse et al., 2014).

Alpine regions in Europe, characterized by rugged terrain and sensitive ecosystems, face escalating risks from intensified rainfall and associated hazards such as landslides and flash floods. Research in countries like Switzerland and Austria emphasizes the need for integrated risk management strategies that consider both upstream land use practices and downstream

vulnerabilities. In Switzerland, the annual cost of flood damage is estimated to be around 1.1 billion Swiss Francs (Bogaard et al., 2020).

Low- and middle-income countries across Latin America, Asia, and Africa are particularly vulnerable to the socio-economic impacts of brief, severe rain events, given their limited resources and inadequate infrastructure. Case studies from countries like Brazil, India, and Nigeria highlight the disproportionate burden borne by marginalized communities, who often lack access to basic services and are more susceptible to displacement and loss of livelihoods (World Bank, 2020; Liu et al., 2018). In Brazil, for example, the economic losses from extreme weather events, including intense rainfall, amount to approximately 0.5% of GDP annually (World Bank, 2020).

Italy, like many other countries, experiences socio-economic impacts from short-duration, high-intensity rainfall events. In regions prone to flooding, such as the Po Valley, extreme rainfall can lead to agricultural losses, damage to infrastructure, and disruptions in economic activities. For example, in Emilia-Romagna, a region in northern Italy, the annual economic cost of flood damage exceeds €300 million (United Nations Development Programme, 2020). Additionally, coastal areas like Venice face unique challenges, with increased rainfall contributing to the ongoing issue of high water, which threatens historic buildings, tourism, and local businesses.

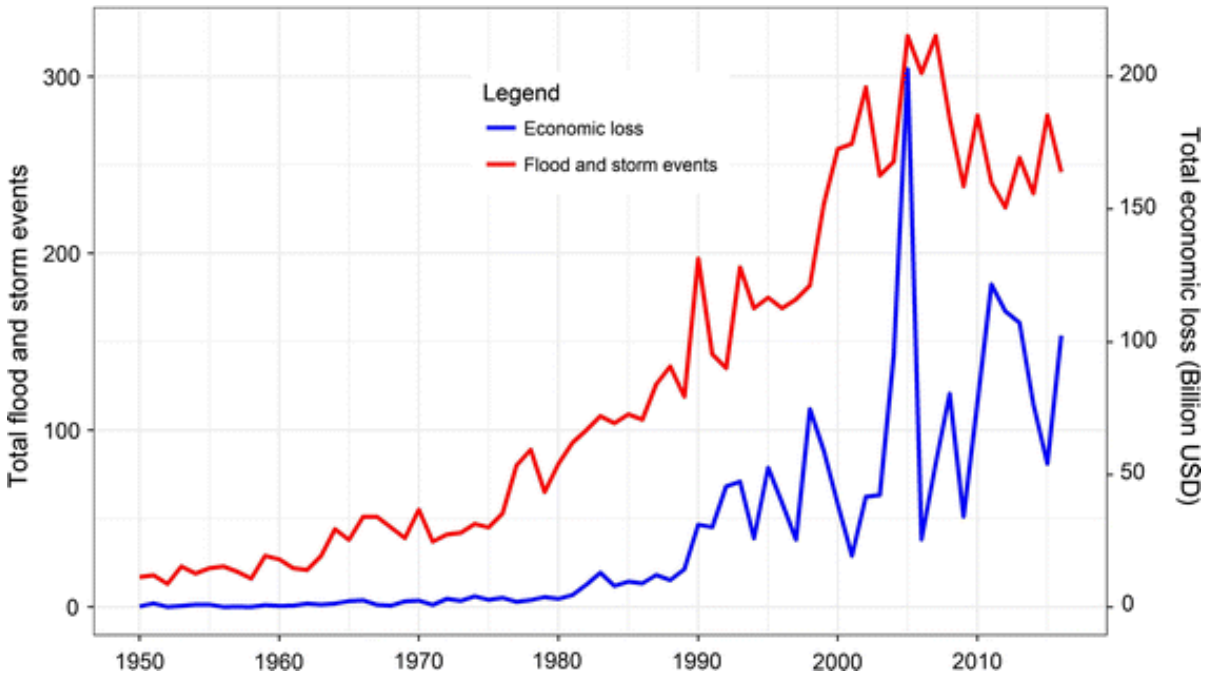

Figure 1.2: Relationship between extreme hydrological events and economic loss.

The Figure above is remarkable in illustrating the incapability to cope with these extreme events to mitigate the economic loss associated with them. For this reason, it is crucial to endeavor to predict and understand the patterns of rainfall. Enhanced investment in predictive technologies and climate models can provide valuable foresight into the timing and intensity of these events, allowing for better-preparedness and response strategies (Taguchi et al., 2019).

1.4 HYPOTHESIS AND GOAL OF THE PRESENT RESEARCH

Building upon the established understanding of climate change impacts on precipitation patterns, this thesis posits that the primary alteration observed in recent precipitation trends is a change in the distribution of rainfall events rather than a significant change in the total quantity of rainfall. Specifically, this research hypothesizes that short-duration rainfall events are increasing at a faster rate compared to longer-duration events.

This hypothesis is supported by a growing body of contemporary research. This phenomenon is becoming increasingly important in modern climate studies due to its implications for urban planning, infrastructure, and flood management. Several studies highlight the disproportionate rise in short-term precipitation intensity due to climate warming.

It has been observed (Ban et al.,2015) that short-term summer precipitation increases more rapidly than longer-term rainfall in their climate models, indicating a heightened sensitivity of brief, intense rain events to temperature increases.

This aligns with findings that projected future intensification of hourly precipitation extremes (Prein et al.,2017), suggesting that short-duration events will become significantly more severe, posing greater risks for flash floods and urban drainage systems.

Further supporting this, It was recently discussed the concept of "super Clausius-Clapeyron scaling," (Lenderink et al.,2017) as we mentioned earlier in this document, where observed increases in extreme hourly convective precipitation exceed the expected rate based on temperature increases alone.

This phenomenon underscores the unique vulnerability of short-duration rainfall to climate change, with short-term precipitation responding more robustly to warming than longer-term events

A comprehensive study by Villarini emphasizes the need for international coordination and high-resolution data to better understand and project these changes (Villarini et al.,2021).

The INTENSE project, under the GEWEX Hydroclimatology Panel, has been pivotal in advancing scientific knowledge of short-duration rainfall extremes by promoting the use of convection-permitting climate models and detailed observational datasets.

This project has shown that localized heavy short-duration rainfall can scale at higher rates than longer-term precipitation, particularly in response to convective storm dynamics.

These findings are not isolated. Research has shown similar trends globally, including in Europe, North America, and Asia. For example, Berg et al. demonstrated a strong increase in convective precipitation with rising temperatures in Europe (Berg et al., 2013) , consistent with researches that revealed heavier summer downpours in the UK with climate change and (Kendon et al., 2014) .

However, studying these trends in Italy poses specific challenges due to the scarcity of high-resolution, short-duration rainfall data. The lack of such detailed observational data hinders the ability to analyze and predict changes in short-term precipitation patterns accurately.

To rigorously test these hypotheses, this thesis will utilize an extensive and detailed dataset provided by the Autonomous Province of Trentino, that have the exceptional characteristic of proving observations at an extremely high temporal resolution, 5 minutes. By capturing the minute-by-minute variations in precipitation, it allows for a thorough and precise analysis of short-duration rainfall events, which are often missed in datasets with longer observation intervals.

By confirming and elucidating the trend towards increasing short-duration rainfall, this research aims contribute to the broader knowledge base required for developing robust climate adaptation and mitigation strategies. Additionally, the unique dataset from Trentino serves as a model for other regions, demonstrating the value of high-resolution precipitation monitoring in climate research.

2: DATA SOURCE AND LIMITATION

2.1 DATA COLLECTION

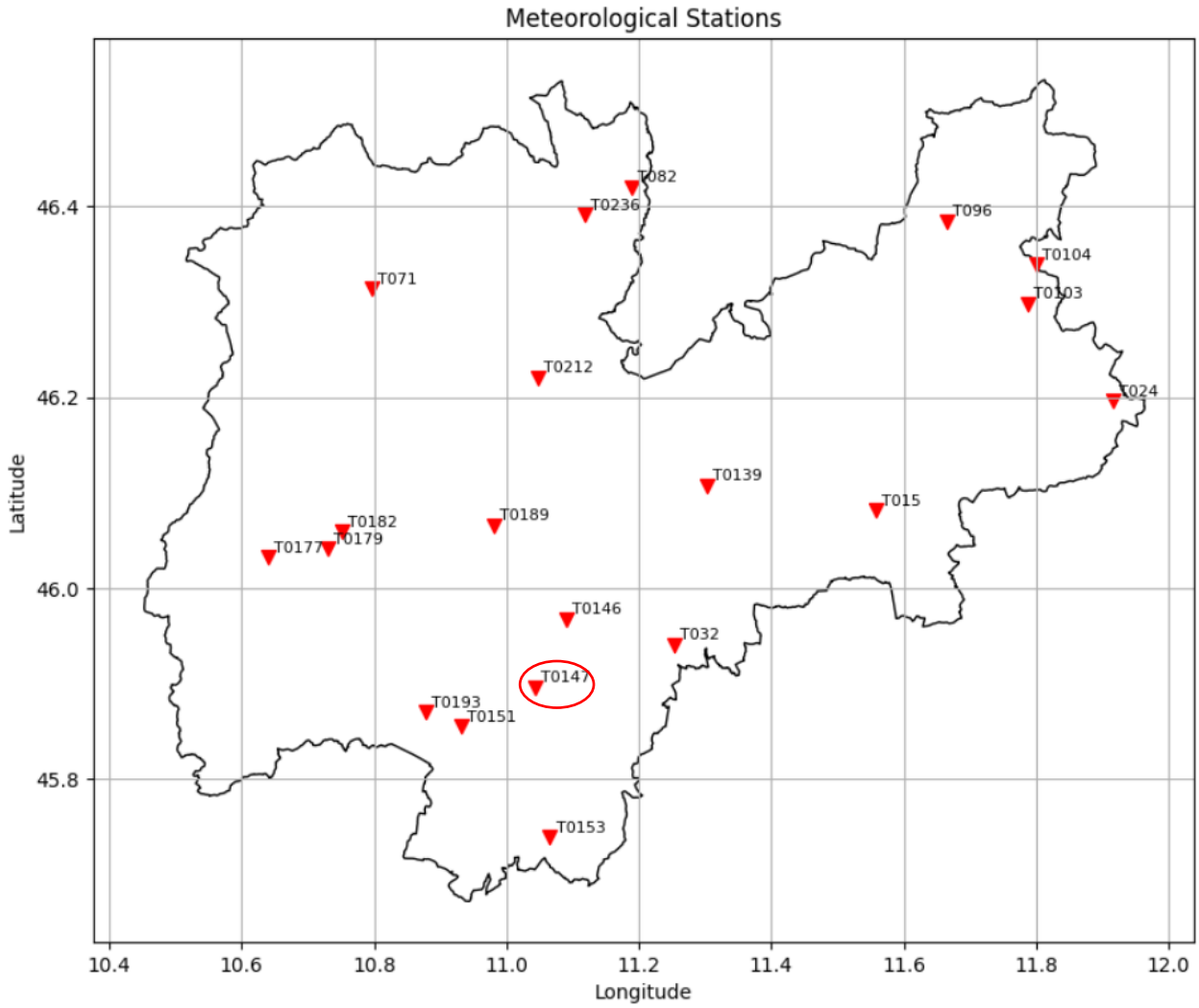

Figure 2.1: Map illustrating the position of the selected weather stations

The data utilized in this study were sourced from the Province of Trentino, an area distinguished by its extensive and detailed meteorological datasets. The region published an exceptionally detailed and rich dataset, particularly with data available at five-minute intervals, characteristic that make it unique in Italy. This region hosts 207 weather stations, each contributing to a rich repository of meteorological information that is accessible for research and analysis. Not only the rainfall observations were extracted from the repository but also the mean values of temperature across the period taken in exam. For this last point

the reasoning behind the choice of taking just one series of temperature value is because of the inconsistency and unavailability of temperature observations in the data source.

Station T0147 is highlighted in the map for two distinct reasons:

- It was selected in order to exploit graphical visualization, that takes place in the next chapter.

- It was chosen to take the values of mean temperature, that were used as covariate in the models fitted for the dissertation.

To facilitate this study, the data were downloaded in CSV file format, with various time resolutions available for selection. These files were then imported into a Python environment, which was employed to manipulate and analyze the data efficiently.

Before delving into the analysis, a thorough preliminary examination of all available weather stations was performed. This meticulous pre-analysis phase involved evaluating multiple aspects such as the quality, consistency, and completeness of the data provided by each station. After a comprehensive review, 24 weather stations were selected for inclusion in the study. These stations were chosen based on the exceptional quality and reliability of their data, ensuring the integrity and accuracy of the research findings. Weather stations that did not meet the stringent criteria were excluded from further analysis to maintain high standards of data integrity.

	NAME	IDENTIFIER	ALTITUDE
1	Ala (Ronchi)	T0153	692m
2	Aldeno (San Zeno)	T0146	182m
3	Bieno	T015	843m
4	Lavarone (Chiesa)	T032	1155m
5	Mezzana	T071	905m
6	Moena (Diga Pezze)	T096	1205m
7	Montagne (Larzana)	T0182	955m
8	Mori (Loppio)	T0151	230m
9	Passo Cereda	T024	1322m
10	Passo Mendola	T082	1315m
11	Passo Rolle	T0103	2012m
12	Passo Valles	T0104	2032m
13	Romeno	T0236	958m
14	Rovereto	T0147	203m
15	Sant'Orsola Terme	T0139	925m
16	Santa Massenza (Centrale)	T0189	252m
17	Spormaggiore	T0212	555m
18	Tione	T0179	533m
19	Torbole (Belvedere)	T0193	90m
20	Val di Breguzzo (Ponte Arno)	T0177	1148m

A critical factor in the selection process was the availability of data at a five-minute resolution, as well as the consistency of the data over a significant period.

Specifically, the selected stations provided continuous data spanning from 1992 to 2023.

Unfortunately, before 1992 it was complicate to find consistency across different stations.

Additionally, another crucial consideration was to choose stations that were well spread across the territory of Trentino, ensuring representation from various geographical locations within the region.

2.2 DATA PROCESSING (ANNUAL MAXIMA)

To ensure thorough analysis and interpretation, meticulous preprocessing was undertaken to organize raw data into structured datasets.

From the original data frames annual maxima were derived. The rationale behind this choice is linked with the scope of the dissertation, that is to investigate about extreme rainfall. To do that, methodologies belonging to the Extreme Value Theory (EVT), a branch of statistics dealing with the stochastic behavior of the extreme values in a process, were employed.

Of the two fundamental approaches pertaining to this branch, the block maxima (BM) method was chosen to run the analysis. This method consists of dividing the observation period into non overlapping periods of equal size and focus the attention on the maximum value of each period. These derived observations follow approximately an extreme value distribution, $G(X)$ (Ferreira et al, 2015).

For the purpose of the research, for each station the block maxima and therefore the subsequent analysis were conducted on three different temporal resolution, aggregated from the same data:

- five minutes interval
- hourly summaries
- daily aggregation.

This multi-resolution approach not only facilitates a nuanced exploration of meteorological phenomena across different time scales but also enhances the detection of subtle patterns and trends that might otherwise evade notice.

2.3 LIMITATIONS OF THE DATA

While the data made available by the Trentino Environment Agency is unique in its high resolution, its potential usefulness is hindered by some limitations which are here explored.

One of the primary concerns is the sample size. As previously highlighted, the analysis spans a period from 1992 to 2023. Deriving annual maxima from the original dataset, means to have data frame that contains only 31 observation each. The limited sample size for annual or multi-annual extremes is a significant constraint and may lead to uncertain statistical results. In fact, despite the fact that the minimum satisfying sample size highly depends on the modeling that needs to be carried on it, A study that analyzes this particular topic identifies the minimum sample size needed to model an extreme value distribution with 25 observations, so the available data frames are slightly over this threshold. However, the same study through a simulation shows that fitting the model on 40 observations lead to similar results compared to the model fitted on 200 observations, obviously on the same data (Cai & Hames, 2010).

This issue is rooted in the data quality and availability before 1992, which was notably poor. Due to the lack of high-quality data from earlier periods, there is no practical way to extend the dataset further back in time. This limitation inevitably introduces uncertainty into the reliability of future scenario modeling based on these extremes.

Within the full dataset, most observations have been validated, ensuring a high level of accuracy. However, there were a few data points with significant uncertainties. These were excluded to prevent any potential noise from skewing the results. The rationale behind this decision lies in the fact that these uncertain data points were relatively insignificant when compared to the already considerable amount of missing data.

Missing data is another crucial issue to consider. Trentino stands out as the only region in Italy providing high-resolution temporal observations, which are essential for detailed meteorological analysis. Unfortunately, even within this region, the datasets suffer from a high percentage of missing data, as highlighted in the table below. This prevalence of missing data poses a substantial challenge, impacting the comprehensiveness and reliability of the analysis.

	NAME	IDENTIFIER	PCT. OF MISSING OBS.
1	Ala (Ronchi)	T0153	50.87%
2	Aldeno (San Zeno)	T0146	51.30%
3	Bieno	T015	48.78%
4	Lavarone (Chiesa)	T032	48.80%
5	Mezzana	T071	49.55%
6	Moena (Diga Pezze)	T096	48.95%
7	Montagne (Larzana)	T0182	53.98%
8	Mori (Loppio)	T0151	52.48%
9	Passo Cereda	T024	49.86%
10	Passo Mendola	T082	50.26%
11	Passo Rolle	T0103	49.03%
12	Passo Valles	T0104	52.01%
13	Romeno	T0236	46.62%
14	Rovereto	T0147	49.22%
15	Sant'Orsola Terme	T0139	49.03%
16	Santa Massenza (Centrale)	T0189	48.90%
17	Spormaggiore	T0212	53.30%
18	Tione	T0179	48.19%
19	Torbole (Belvedere)	T0193	49.70%
20	Val di Breguzzo (Ponte Arno)	T0177	52.28%

Typically, with such a significant amount of missing information, making reliable statistical assumptions becomes challenging. However, considering also our previous discussion about the sample size, our primary interest lies not in the precise numerical values but in understanding the behavior and patterns of rainfall. We aim to explore trends, rates of change, and data distributions.

With this perspective, and assuming that the missing data are randomly distributed and do not follow any specific pattern, the analyses conducted on the available data can still be

considered reliable. This approach allows us to extract meaningful insights into rainfall behavior despite the inherent limitations.

2.4 DESCRIPTIVE STATISTIC

For the analysis in this dissertation, two programming languages were employed:

- Python: This language served as the primary tool for all data manipulation, exploratory data analysis, and visualization tasks.
- RStudio: It was utilized to fit models to the distribution, facilitating the importation of pre-processed data from Python.

Before embarking on the methodology analysis, extensive exploratory analyses were conducted on the available stations, on the annual maxima data frames directly, given that the research emphasis on extremes and their distributional behavior, rather than the entire dataset.

In order to comprehend the main characteristics of the available data, descriptive statistics were computed for all different time resolutions as outlined below.

5 MINUTES

	Station	Median	Std Dev	CV	Mean	75th Percentile	90th Percentile	Skewness
1	T0153	7.400000	2.093914	27.942138	7.493750	8.850000	9.200000	0.652444
2	T032	7.900000	2.289386	28.979575	7.900000	9.650000	10.380000	-0.158046
3	T0146	7.400000	2.741254	33.764489	8.118750	9.450000	11.680000	0.814807
4	T015	8.700000	2.482706	28.847713	8.606250	10.000000	11.960000	0.571422
5	T071	4.700000	1.523353	33.526342	4.543750	5.650000	6.180000	-0.305933
6	T096	6.700000	1.955874	28.016102	6.981250	8.200000	8.780000	0.510394
7	T0182	7.200000	3.721407	49.208689	7.562500	8.650000	11.520000	1.896785
8	T0151	7.800000	1.863703	25.227784	7.387500	9.000000	9.400000	-0.528622
9	T024	6.700000	2.225068	32.691540	6.806250	8.500000	9.400000	-0.352270
10	T082	7.000000	2.636645	36.025888	7.318750	9.050000	10.700000	0.473980
11	T0103	5.800000	2.187907	35.793974	6.112500	7.200000	9.520000	0.606479
12	T0236	6.600000	2.126096	30.953165	6.868750	7.600000	9.580000	0.743404
13	T0147	7.900000	3.259620	36.805869	8.856250	10.500000	13.760000	0.724011
14	T0139	7.200000	3.598247	44.048926	8.168750	8.900000	11.160000	2.536326
15	T0212	6.100000	2.266410	37.384077	6.062500	7.450000	8.780000	-0.275198
16	T0179	7.200000	2.106968	29.859601	7.056250	7.850000	10.420000	0.800342
17	T0104	5.200000	1.922196	35.432190	5.425000	6.250000	7.160000	0.842751
18	T0189	8.000000	2.427931	30.816046	7.878788	9.200000	10.920000	-0.407739
19	T0193	7.700000	2.588187	30.903720	8.375000	10.350000	11.980000	0.417739
20	T0177	6.700000	2.750718	41.677551	6.600000	8.050000	10.540000	0.595307

Figure 2.2: Descriptive statistics for 5 minutes Stations

Examining the central tendency and spread of the data, we observe that the mean values across the stations range from approximately 4.54 mm (Station T071) to 8.86 mm (Station T0147), with most stations having means between 6 and 8 mm. The median values are generally close to the mean values, indicating that the data distributions are relatively symmetric for many stations. This close alignment between mean and median suggests a balanced distribution without significant skew in many cases.

In terms of variability, the standard deviation values highlight significant differences within the data. Station T0182 shows the highest variability with a standard deviation of 3.72 mm,

suggesting wide fluctuations in its measurements. Conversely, Station T071 exhibits relatively low variability with a standard deviation of 1.52 mm, indicating more consistent readings.

The coefficient of variation (CV), which standardizes the standard deviation relative to the mean (CV = $\frac{\sigma}{\mu} * 100$), further elucidates these differences. Station T0182 has the highest relative variability (CV = 49.2%), indicating significant spread compared to its mean. In contrast, Station T0151 has the lowest CV (25.23%), suggesting more consistency in its measurements.

75th percentile and 90th percentile provide insights into the distribution's upper range. For instance, Station T0103 has a 90th percentile value of 9.52 mm, indicating that 90% of the measurements are below this value. On the other hand, Station T0139 has a notably high 90th percentile value of 11.16 mm, suggesting occasional extreme measurements.

Skewness values further reveal the asymmetry of the data distribution. Positive skewness, such as that seen in Station T0139 with a skewness of 2.54, indicates a longer right tail. This suggests occasional high values far from the mean, which can be critical for understanding potential extreme events. Conversely, negative skewness, such as that observed in Station T032 with a skewness of -0.16, suggests a longer left tail, indicating more frequent low values.

1 HOUR

	Station	Median	Std Dev	CV	Mean	75th Percentile	90th Percentile	Skewness
1	T0153	23.900000	8.494666	33.476517	25.375000	32.800000	34.120000	0.261316
2	T032	26.900000	11.402035	39.598994	28.793750	33.300000	43.720000	1.018023
3	T0146	22.900000	8.670147	34.802397	24.912500	29.800000	37.560000	0.785988
4	T015	24.600000	8.063636	31.292304	25.768750	28.900000	37.680000	0.805989
5	T071	12.800000	5.615987	38.982993	14.406250	17.400000	20.680000	1.581288
6	T096	22.000000	11.542956	47.624368	24.237500	27.450000	36.160000	1.674791
7	T0182	21.100000	11.067810	48.160173	22.981250	27.400000	32.020000	2.587513
8	T0151	23.300000	6.062121	24.661566	24.581250	28.450000	31.520000	0.462994
9	T024	25.800000	8.381816	32.331016	25.925000	30.650000	36.880000	0.315727
10	T082	24.200000	8.943350	35.586570	25.131250	29.700000	34.960000	0.624313
11	T0103	24.400000	16.284482	60.962029	26.712500	29.500000	37.660000	3.320577
12	T0236	20.100000	7.324217	34.175407	21.431250	26.000000	32.440000	0.606804
13	T0147	23.200000	12.753619	46.813009	27.243750	30.850000	39.960000	1.759115
14	T0139	25.900000	8.137964	30.224563	26.925000	30.350000	37.240000	0.786732
15	T0212	17.500000	7.744540	41.553536	18.637500	23.250000	31.160000	0.328877
16	T0179	20.300000	8.210062	36.992677	22.193750	23.450000	35.560000	1.069986
17	T0104	19.600000	6.948842	33.559155	20.706250	24.200000	25.180000	2.005933
18	T0189	21.200000	8.382083	34.645654	24.193750	29.200000	37.660000	0.472448
19	T0193	25.100000	8.195002	31.189353	26.275000	31.400000	35.560000	0.718244
20	T0177	21.000000	24.446929	88.323699	27.678788	29.400000	44.440000	3.494334

Figure 2.3: Descriptive statistics for 1 hour Stations

The mean values across the stations range from around 14.41 mm (Station T071) to 28.8 mm (Station T032). Most stations have means between 20 and 28 mm. As for the 5 minutes time resolution the median values are generally close to the mean values.

Regarding variability, the standard deviation values show significant differences within the data. Station T0177 has the highest variability with a standard deviation of 24.45 mm, and a coefficient of variation of 88.32% indicating wide fluctuations in its measurements. Conversely, Station T0151 shows relatively low variability with a standard deviation of 6.06 mm (CV = 24.66%), suggesting more consistent readings.

Examining the percentiles, Station T0177 has a 90th percentile value of 44.44 mm, meaning that 90% of the measurements are below this value. On the other hand, Station T032 has a high 90th percentile value of 43.72 mm, suggesting occasional extreme measurements. These percentile values help understand the typical upper range of the data and identify stations with potential outliers.

Skewness values further indicate the asymmetry of the data distribution. Positive skewness, such as that seen in Station T0177 with a skewness of 3.49, points to a longer right tail. This indicates occasional high values far from the mean. Conversely, negative skewness is not observed in this dataset, indicating that all stations show a tendency towards higher values rather than lower ones.

1 DAY

	Station	Median	Std Dev	CV	Mean	75th Percentile	90th Percentile	Skewness
1	T0153	86.000000	32.173592	35.570582	90.450000	108.250000	125.420000	1.030636
2	T032	103.200000	40.530425	39.995485	101.337500	125.275000	149.260000	0.456595
3	T0146	60.800000	14.955914	24.608661	60.775000	70.000000	77.720000	0.756984
4	T015	72.800000	24.916891	32.187167	77.412500	95.900000	108.860000	0.431692
5	T071	63.200000	18.666192	30.990876	60.231250	73.100000	82.760000	0.141459
6	T096	50.700000	22.039956	38.600985	57.096875	68.650000	79.480000	1.886828
7	T0182	69.200000	29.919537	39.809778	75.156250	95.550000	99.800000	1.162641
8	T0151	63.400000	17.953108	27.013658	66.459375	76.225000	89.240000	0.773172
9	T024	102.300000	70.115158	56.554459	123.978125	143.900000	212.540000	1.737459
10	T082	55.150000	18.176766	30.937531	58.753125	74.225000	81.080000	0.229894
11	T0103	79.700000	29.215213	33.899732	86.181250	104.950000	132.000000	0.483493
12	T0236	57.500000	20.599756	33.560340	61.381250	74.050000	82.590000	0.807952
13	T0147	59.700000	15.217539	25.664660	59.293750	69.275000	77.140000	0.779735
14	T0139	62.000000	27.530647	40.525355	67.934375	80.850000	99.800000	1.117820
15	T0212	67.700000	26.717150	37.272159	71.681250	94.200000	99.340000	-0.016128
16	T0179	70.450000	22.835410	30.933121	73.821875	97.200000	104.320000	0.173818
17	T0104	73.800000	25.240650	32.283496	78.184375	92.100000	109.760000	0.783977
18	T0189	54.800000	21.018062	35.378360	59.409375	68.700000	94.980000	0.973083
19	T0193	56.900000	19.649799	32.840317	59.834375	70.900000	77.130000	1.438258
20	T0177	73.600000	32.553043	41.571449	78.306250	96.750000	126.420000	0.625056

Figure 2.4: Descriptive statistics for 1 day Stations

The mean values across the stations range from approximately 59.41 mm (Station T0189) to 123.98 mm (Station T024), with most stations having means between 60 and 100 mm. The data distributions are relatively symmetric for many stations.

Standard deviation values reveal considerable differences within the data. Station T024 shows the highest variability with a standard deviation of 70.12 mm (CV = 56.55%), indicating wide fluctuations in its measurements. Conversely, Station T0147 exhibits relatively low variability with a standard deviation of 15.22 mm.

3 METHODOLOGIES

The chapter will initially focus on the rigorous methodology applicated to the whole data available.

The second part of the chapter will focus on the graphical visualization of the research and the methods. Due to the vast array of datasets utilized in the research, for clarity purposes, a single station was selected as an exemplar. This station was chosen for its representativeness in the studied phenomena, with a particular focus on the 5-minute temporal resolution, which constitutes our primary interest.

3.1 TREND AND SLOPE ANALYSIS

The analysis were conducted following different researches and studies that share a common approach in evaluating rainfall extremes. This approach consists in using Mann-Kendall test, Theil-Sen Slope estimator and GEV distributions (Aditya et al., 2021; Gadedjisso-Tossou et al., 2021; Sudarsan & A, 2023).

The initial step involves assessing the presence of a monotonic trend in the annual maxima time series. To achieve this, the non-parametric Mann-Kendall test (Yue & Wang, 2004) has been employed across all stations. This statistical test serves to detect trends in time series data, particularly useful when the data does not conform to a normal distribution or exhibits serial correlation among data points.

The Mann-Kendall test operates by comparing the ranks of data points over time, providing a straightforward means of trend detection without making assumptions about the distribution of the data.

The test statistic S of the Mann-Kendall test can be expressed as follows:

$$S = \sum_{i=1}^{n-1} \sum_{j=1+1}^{n} sign(Xj - Xi)$$

Where:

- n is the number of data points in the time series.
- Xj and Xj are data points at positions i and j n the time series, respectively.

$sign(Xj - Xi)$ is the sign function, which returns:

- +1 if $Xj > Xi$,
- -1 if $Xj < Xi$,
- and 0 if $Xj = Xi$

The test statistic S reflects the overall pattern of increasing or decreasing values in the time series.

Kendall's tau τ is then derived from the test statistic S and is defined as:

$$\tau = \frac{S}{\frac{1}{2}n(n-1)}$$

Where n is the number of the data points in the time series. Kendall's tau quantifies the degree of concordance (or discordance) between the ranks of data pairs in the time series.

A positive tau indicates a tendency for data pairs to have the same order over time, suggesting an increasing trend, while a negative tau indicates the opposite.

Following the Mann-Kendall test, which assesses the presence of a monotonic trend, the Theil-Sen estimator is employed to investigate the magnitude of the trend. (Sen, 1968)

While simple linear regression was considered as a method, the Theil-Sen estimator was chosen due to its non-parametric nature. This characteristic renders it devoid of assumptions about the distribution of the data, making it robust and resistant to outliers.

In the Theil-Sen estimator, the slope is computed as the median of the slopes between all pairs of sample points, while the intercept is calculated as the median of the differences between the observed values and the slopes at each point.

The slope b is thus calculated as follows:

$$b = median\ \frac{X_j - X_i}{t_j - t_i}\ for\ all\ i < j, i = 1,2, \dots, (n-1), j = 2,3, \dots, n$$

Where, X_i and X_j are the annual maximum rainfalls for years $t_i$and t_j respectively.

The intercept b_0 is calculated as:

$$b_0 = X_i - bt_i$$

3.2 GEV ANALYSIS

After assessing the trends it's imperative to delve into the distribution of the data, aiming to model it as accurately as possible to comprehend its behavior.

Given our focus on rare values, Extreme Value Theory emphasizes meticulous modeling of the tails of the distribution. To achieve this, the Generalized Extreme Value Distribution (GEV) emerges as a fundamental distribution capable of capturing the data's behavior (Kotz & Nadarajah, 2000).

It roots his theoretical justification from the Three Types Theorem (Coles, 2001), stated by Fisher and Tippett and later derived rigorously by Gnedenko.

This theorem affirms that if a nondegenerate H exists (distribution function which does not put all its mass at a single point) it must be one of the three types:

$$H(x) = exp(-e^{-x}), \qquad all\ x$$

$$H(x) = \begin{cases} 0, & x < 0 \\ \exp(-x^{-\alpha}, & x > 0 \end{cases}$$

$$H(x) = \begin{cases} \exp(-|x|^{\alpha}), & x < 0 \\ 1, & x > 0 \end{cases}$$

Which are often referred, respectively as Gumbel type, Fréchet type and Weibull type. These three types can be combined into a single Generalized Extreme Value Distribution.

The Probability Density Function of the GEV distribution can be written as:

$$f(X, \mu, \sigma, \varepsilon) = \frac{1}{\sigma}\left[1 + \varepsilon(\left(\frac{X-\mu}{\sigma}\right)\right]^{-1/\varepsilon - 1} exp\left\{-\left[(1 + \varepsilon\left(\frac{X-\mu}{\sigma}\right)\right]^{-1/\varepsilon}\right\}$$

From the pdf, it can be derived the Cumulative Distribution Function (CDF):

$$G(X) = F(X; \mu, \sigma, \varepsilon) = exp\left\{-\left[1 + \varepsilon\left(\frac{X-\mu}{\sigma}\right)\right]^{-1/\varepsilon}\right\}, \quad \text{with } \left\{X: 1 + \varepsilon\left(\frac{X-\mu}{\sigma}\right) > 0\right\}$$

X is the annual maximum rainfall and μ, σ, ε denote the location, shape and scale parameters.

The location parameter (μ), similarly to the mean of a Normal Distribution, delineates the central tendency or mode of the distribution. Thus, increasing the location parameter shifts the entire distribution to the right, while decreasing it shifts the distribution to the left.

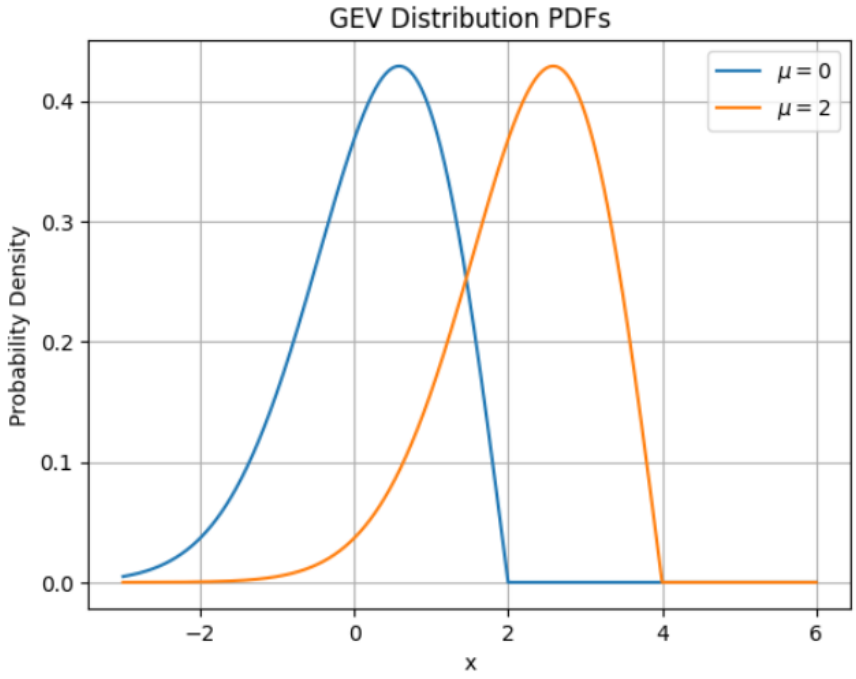

Fig 3.1: Location parameter in GEV Distributions

The scale parameter (σ) regulates the spread and dispersion of the distribution, akin to the role of standard deviation in a Normal Distribution. It signifies the variability around the location parameter.

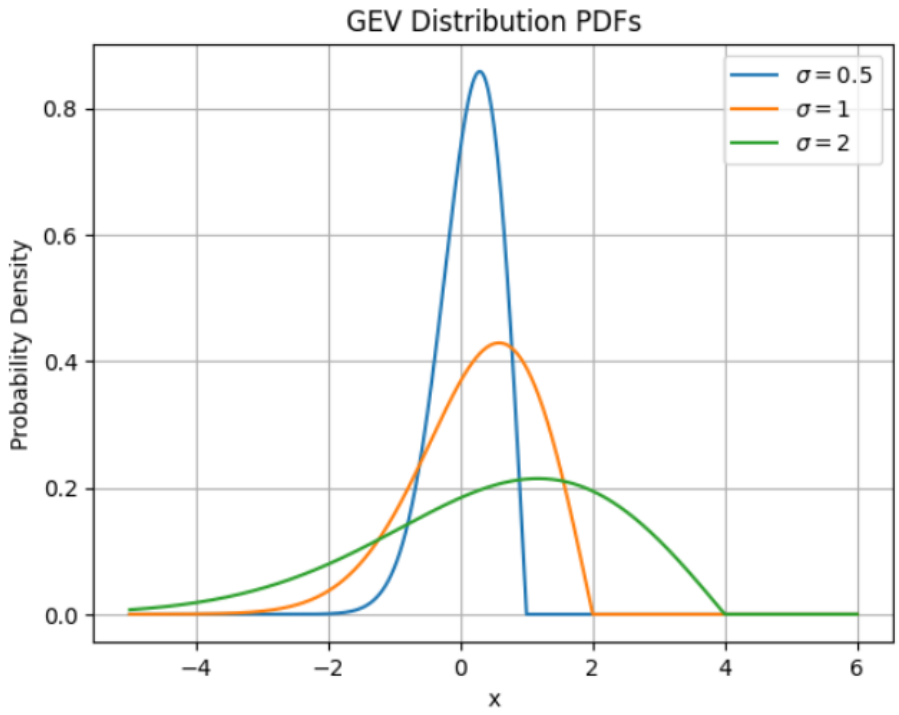

Figure 3.2: Shape parameter in GEV Distributions

The shape parameter (ε) dictates the tail behavior of the distribution, specifically determining the rate at which the tail decays. It influences the extremeness of the distribution and characterizes its long-term behavior.

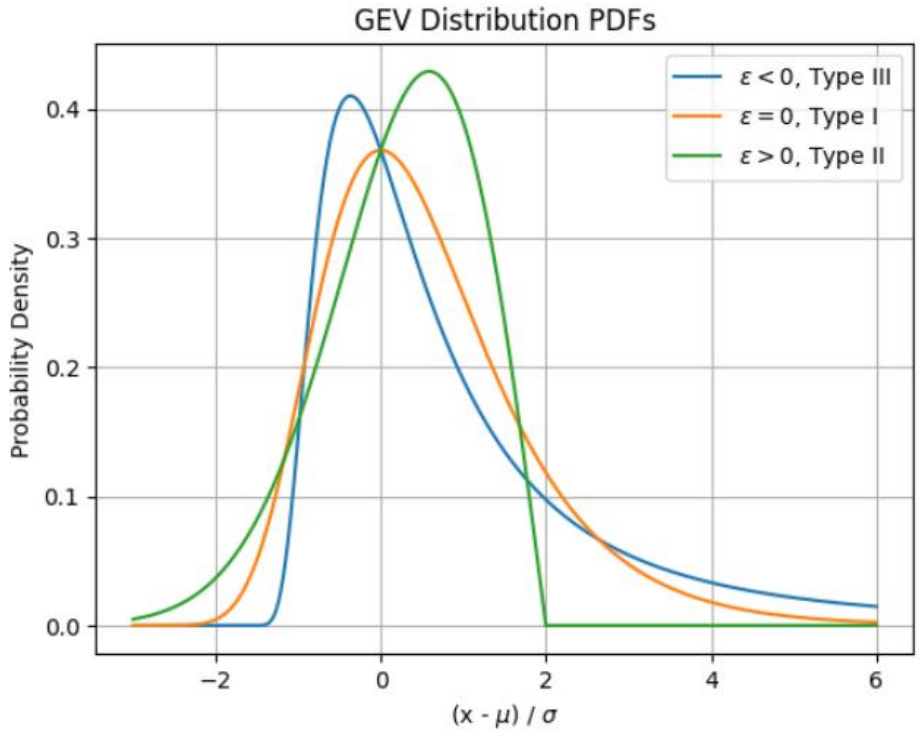

Figure 3.3: Scale parameter GEV Distributions

The shape parameter as well which of the three types the GEV falls into:

- $\varepsilon = 0$ we have a Gumbel Distribution (Type I)
- $\varepsilon > 0$ determines a Fréchet Distribution (Type II)
- $\varepsilon < 0$ corresponds to a Weibull Distribution (Type III)

The above theoretical framework of the GEV distribution refers to a condition of stationarity, meaning that there are no trends in the data, and therefore the parameters of the distribution are kept fixed over time.

But, under the climate change context, the intensity and/or the frequency of extreme rainfall events can change with time, so that the hypothesis of stationarity of the series of annual maxima is not satisfied (De Paola et al., 2018).

For this reason, it arises the necessity to introduce covariates in the model in order to allow parameters to vary.

In the present dissertation, the GEV models are fitted allowing the location parameter to vary, adding two distinct covariates. The most intuitive is the time (Coles, 2001) covariate. GEV models are modeled also considering the mean temperature (Siow et al., 2023) of the area as covariate.

Five different GEV model have been fitted:

(1) A Stationary GEV model, with all the parameters kept fixed.

(2) A non-stationary model, with the location parameter expressed as a linear function of Time:

The location parameter becomes:

$$\mu(t) = \mu_0 + \beta_\mu t$$

Where:

- μ_0 is the baseline location parameter at $t = 0$
- β_μ is the coefficient that describes the linear trend of the location parameter with respect to time t.

Inserting the new location parameter in the cumulative distribution function it becomes:

$$G(X) = F(X; \mu(t), \sigma, \varepsilon) = exp\left\{-\left[1 + \varepsilon\left(\frac{X-(\mu_0+\beta_\mu t)}{\sigma}\right)\right]^{-1/\varepsilon}\right\},$$

with $1 + \varepsilon\left(\frac{X-(\mu_0+\beta_\mu t)}{\sigma}\right) > 0$

(3) A GEV model with quadratic time relationship (Min & Halim, 2020) have been fitted as well.

Adding a quadratic term allow to grasp more complex relationships between the two variables, especially if the relation is not purely linear; similar to the mode just discussed, the location parameter becomes:

$$\mu(t) = \mu_0 + \beta_{\mu 1} t + \beta_{\mu 2} t^2$$

With $\beta_{\mu 2} t^2$ describing the quadratic trend of the location parameter with respect to time t^2.

GEV becomes:

$$G(X) = F(X; \mu(t), \sigma, \varepsilon) = exp\left\{-\left[1 + \varepsilon\left(\frac{X-(\mu_0+ \beta_{\mu 1} t+\beta_{\mu 2} t^2)}{\sigma}\right)\right]^{-1/\varepsilon}\right\},$$

with $1 + \varepsilon\left(\frac{X-(\mu_0+ \beta_{\mu 1} t+\beta_{\mu 2} t^2)}{\sigma}\right) > 0$

(4) Similarly to the first two models, it has been considered the temperature as the covariate, the linear relationship is expressed as:

$$\mu(T) = \mu_0 + \beta_\mu T$$

And therefore the GEV becomes:

$$G(X) = F(X; \mu(T), \sigma, \varepsilon) = exp\left\{-\left[1 + \varepsilon\left(\frac{X-(\mu_0+\beta_\mu T)}{\sigma}\right)\right]^{-1/\varepsilon}\right\},$$

with $1 + \varepsilon\left(\frac{X-(\mu_0+\beta_\mu T)}{\sigma}\right) > 0$

(5) And the quadratic temperature relationship expressed as:

$$\mu(T) = \mu_0 + \beta_{\mu 1} T + \beta_{\mu 2} T^2$$

The GEV becomes :

$$G(X) = F(X; \mu(T), \sigma, \varepsilon) = exp\left\{-\left[1 + \varepsilon\left(\frac{X-(\mu_0 + \beta_{\mu 1}T + \beta_{\mu 2}T^2)}{\sigma}\right)\right]^{-1/\varepsilon}\right\},$$

with $1 + \varepsilon\left(\frac{X-(\mu_0 + \beta_{\mu 1}T + \beta_{\mu 2}T^2)}{\sigma}\right) > 0.$

3.3 MODEL COMPARISON

In order to select the best possible model, two different criteria have been used to assess the goodness of the fit.

(1) Akaike Information Criterion (AIC) computed as:

$$AIC = -2\ ln(L) + 2k$$

Where:

- L is the likelihood of the model given the data.
- $k\ is\ the\ number\ of\ estimated\ parameters\ in\ the\ model$.

(2) Bayesian Information Criterion (BIC):

$$BIC = \ 2\ ln(L) + k\ ln(n)$$

Where:

- L is the likelihood of the model given the data.
- $K\ is\ the\ number\ of\ estimated\ parameters\ in\ the\ model$.
- $n\ is\ the\ sample\ size$

For both criteria, a smaller value indicates a better fit, both have strengths and weaknesses, in general BIC imposes stronger penalty for more complex models.

3.4 GRAPHICAL ANALYSIS

Let's now consider our selected sample station, T0147 in Rovereto, situated at an altitude of 203 meters in the southern region of Trentino. Moving forward, graphical representations will exclusively focus on the 5-minute data frame.

A popular hypothesis tested pertains to seasonal variations, positing that a significant portion of stations demonstrate elevated extreme observations during the summer (Peter et al., 2024) months. Empirical examination of the data overwhelmingly corroborates this hypothesis.

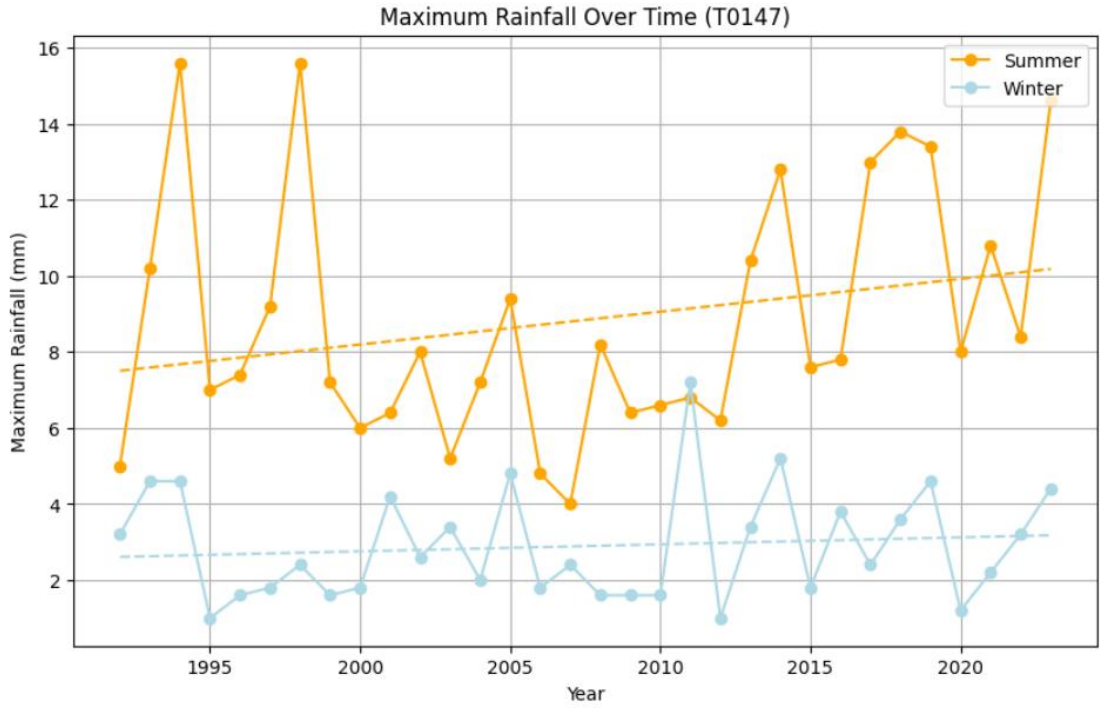

Figure 3.4: Seasonal Annual Extremes

As previously mentioned, our analysis operates within the framework of Extreme Value Theory, specifically concerning the evaluation of extreme events. Therefore, it's imperative to delve into the distribution of the data, aiming to model it as accurately as possible to comprehend its behavior.

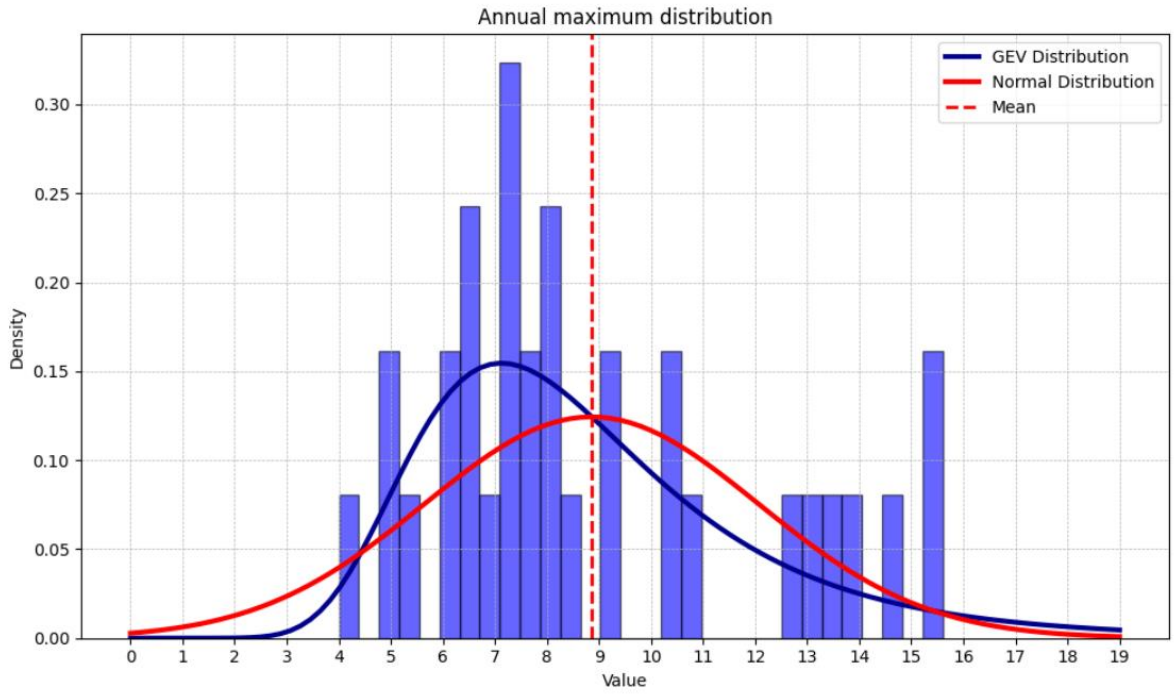

Figure 3.5: Density Histogram with Fitted Distribution for Rovereto Station

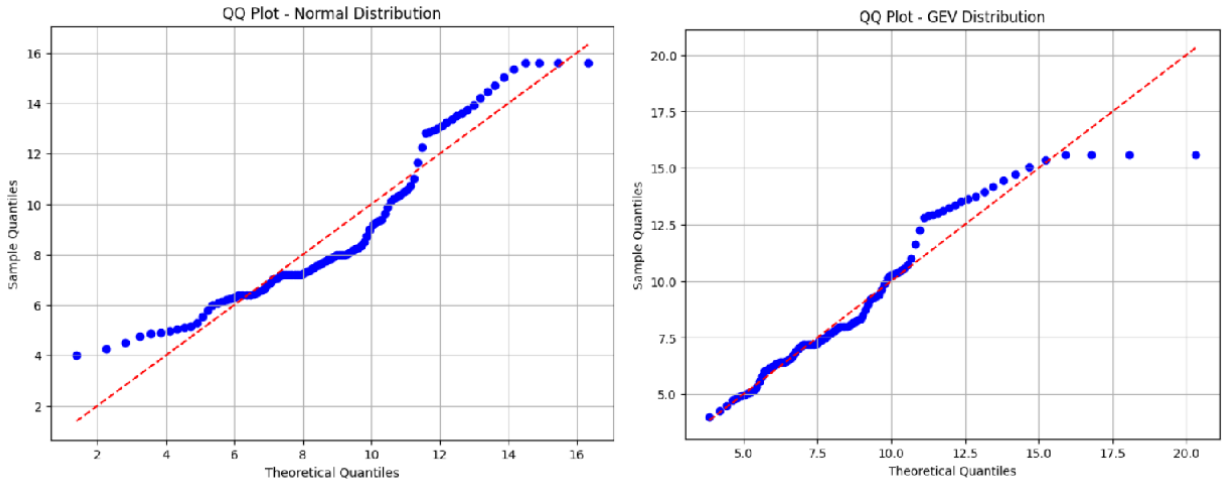

Figure 3.6: Diagnostic Plots, on the left the QQ-Plot associated with the fitted Normal, on the right the QQ-Plot for GEV Distribution

Above there is the density histogram of the selected station for comprehension, with two different distributions fitted to the data: a Normal Distribution for comparison purposes and a stationary GEV distribution. It's evident upon inspection that the red line representing the GEV distribution better aligns with the tails of the histogram, a observation further corroborated by the diagnostic plot.

Having a distribution that accurately fits the data is paramount for making predictions about future scenarios. With the fitted GEV distribution, it becomes feasible to estimate the frequency with which extreme quantiles occur at certain return levels.

The return value is defined as a value that is expected to be equaled or exceeded on average once every interval of time (T) (with a probability of 1/T).

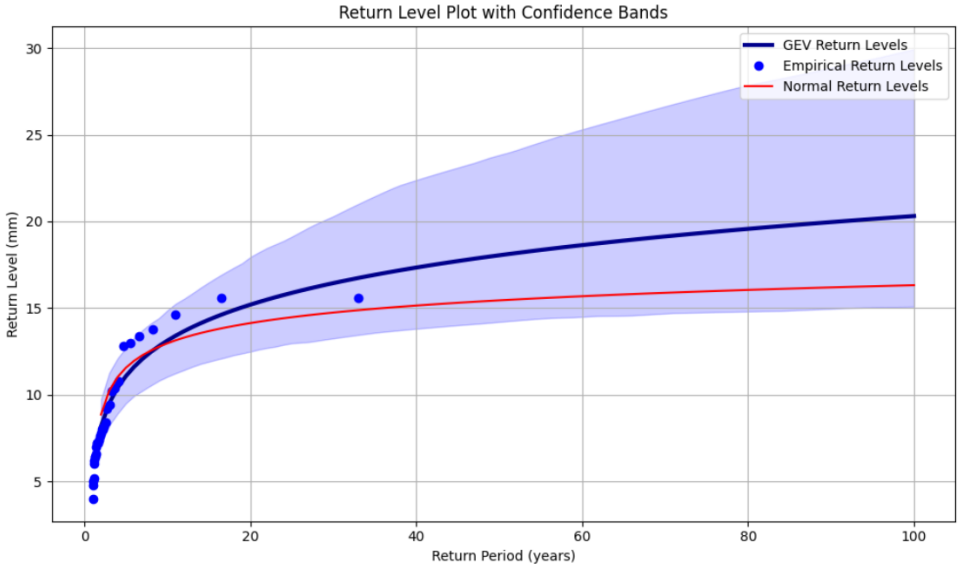

Figure 3.7: Return Levels for T0147 Station, calculated with three different methods

We can see how the return levels change depending on the method used for the calculations, and therefore the importance to fit the best possible GEV model in order to get the more accurate predictions.

The above GEV distribution, and the return plot are referred to a framework of stationarity. But as mentioned this is against theories and findings (Jayaweera et al., 2023) of climatologists all over the world.

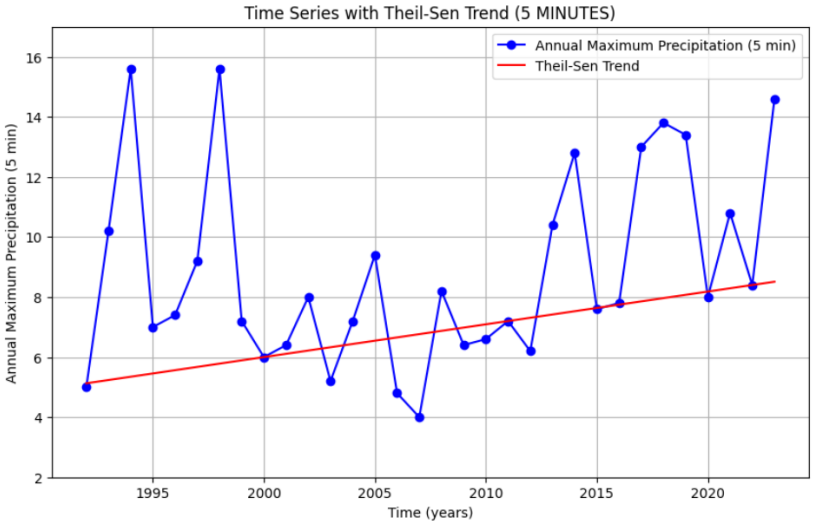

Figure 3.8: Annual maxima with Theil-Sen trend (5 min)

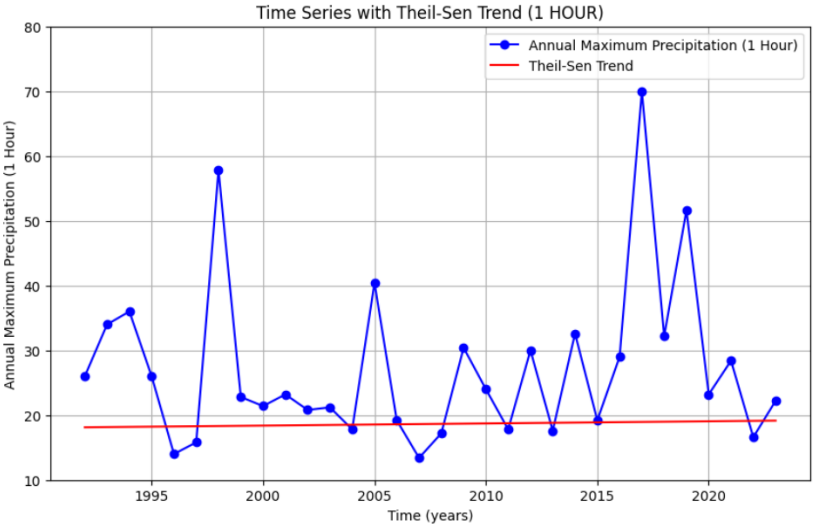

Figure 3.9: Annual maxima with Theil-Sen trend (1 hour)

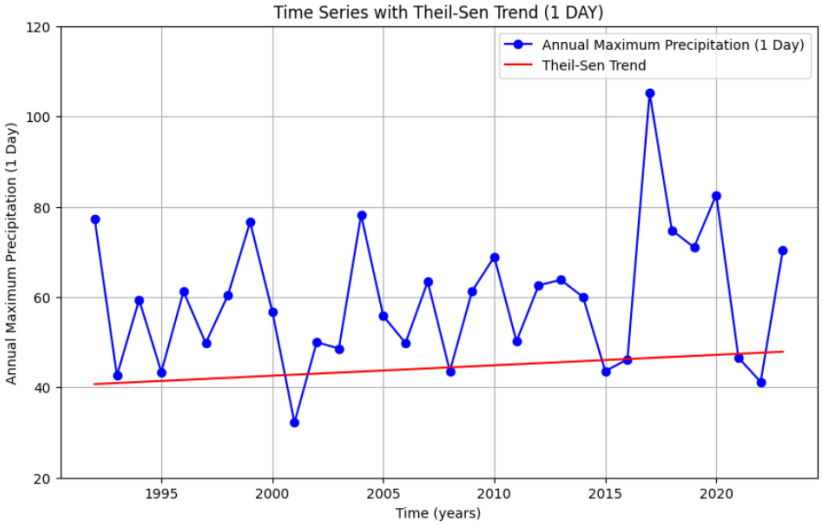

Figure 3.10: Annual maxima with Theil-Sen trend (1 day)

In the plot illustrating the time series for the Rovereto Station across three different time resolutions, it becomes immediately apparent that clear trends are present.

Of note is the steeper trend observed in the time series for the five-minute duration, computed through the Theil-Sen estimator. However, the trend lines for the other durations also exhibit positive slopes, indicating a general increase in rainfall amount for this station.

Typically, the GEV distribution has a stationarity condition, meaning that the parameters μ, σ, ε should remain constant over time and Xt (the annual maxima) is identically distributed (Coles, 2001) for all t (the extremes values does not change with time).

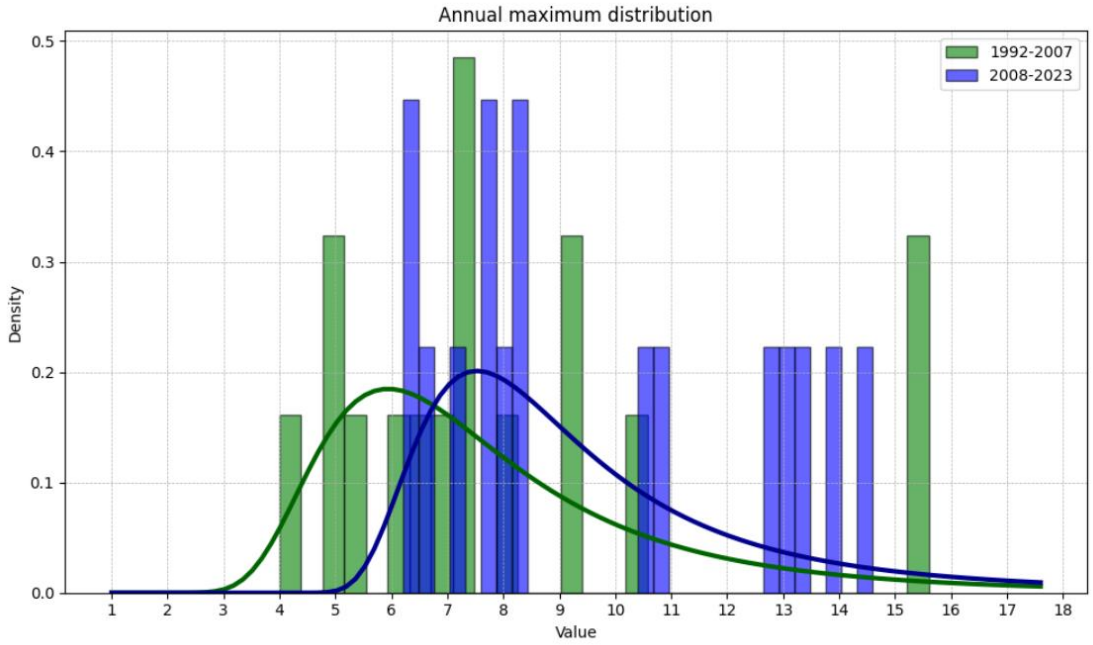

Figure 3.11: Two Period Density Histogram with Fitted distributions

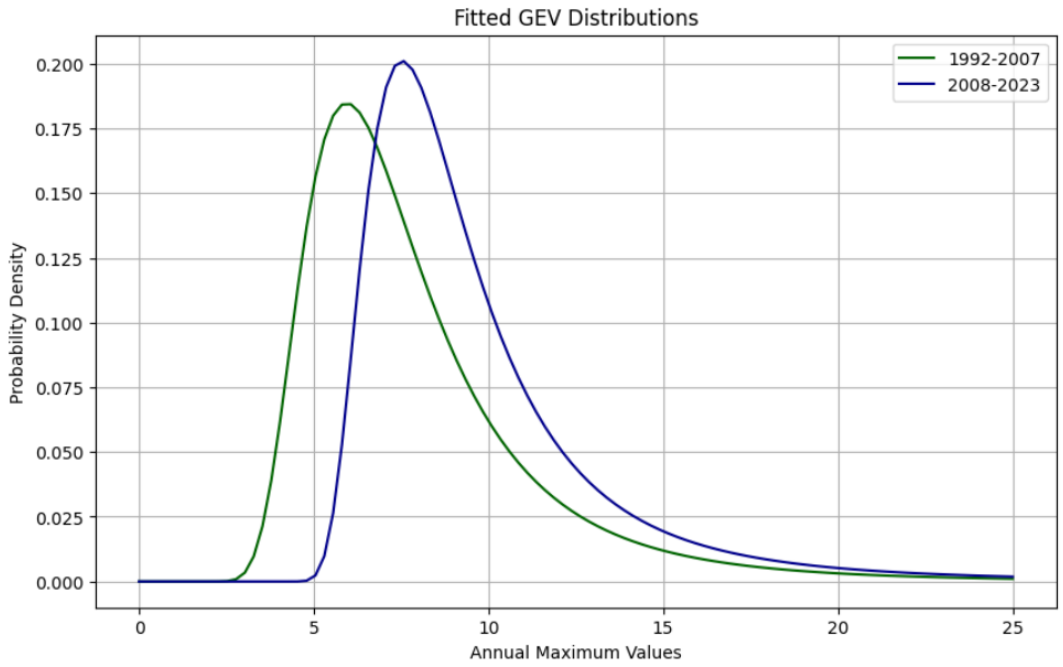

Figure 3.12: Fitted GEV distributions

	Mean	Standard Deviation	Skew
1992-2007	8.0125	3.425760	1.376621
2008-2023	9.7000	2.950254	0.456306

	Shape	Location	Scale
1992-2007	-0.217623	6.333949	2.035376
2008-2023	-0.302405	8.012287	1.907195

Figure 3.13: Two Periods Descriptive Statistics and GEV parameters

Above, the block maxima has been divided into two distinct periods, followed by fitting a GEV distribution to each period. Notably, there is an increase observed in both the mean and location parameters of the GEV distributions.

These observations strongly suggest that the dataset is non-stationary, with the severity of extreme events showing an upward trend. Consequently, in light of the fact that the GEV distribution typically assumes no clear trend in the data, adjustments to the fitting models are imperative. Keeping the parameters fixed would impede a comprehensive understanding of rainfall behavior.

The next logical step involves introducing changes, particularly by incorporating covariates into the parameters of the distribution, thereby allowing them to vary over time. Recalling the significance of the parameters discussed earlier in the dissertation, and drawing insights from

existing literature on this subject, it's pertinent to explore avenues for accommodating these changes.

The shape parameter holds crucial significance in understanding rainfall behavior, as its sign and magnitude dictate the tails of the distribution, thereby modeling the most extreme and potentially destructive events. However, it's common practice to keep this parameter fixed due to the complexity of understanding the underlying phenomena driving its variation, as well as the challenge of finding external covariates that adequately describe this behavior.

Conversely, allowing the scale parameter to vary can capture changes in the variability of the distribution. However, when discussing non-stationarity, the location parameter assumes paramount importance.

As previously discussed, an increase in the location parameter signifies a shift of the distribution to the right, thereby corroborating the hypothesis regarding increasing rainfall extremes. Consequently, allowing the location parameter to vary makes intuitive sense, particularly considering the observed increasing trend in block maxima over time.

In the present dissertation, GEV models are fitted with the flexibility for the location parameter to vary, facilitated by the inclusion of two distinct covariates. The most straightforward covariate is time itself, capturing the temporal evolution of rainfall extremes. Additionally, GEV models are also informed by incorporating the mean temperature of the area as a covariate, enriching the understanding of rainfall behavior.

4 RESULTS

4.1 TREND IN ANNUAL MAXIMA

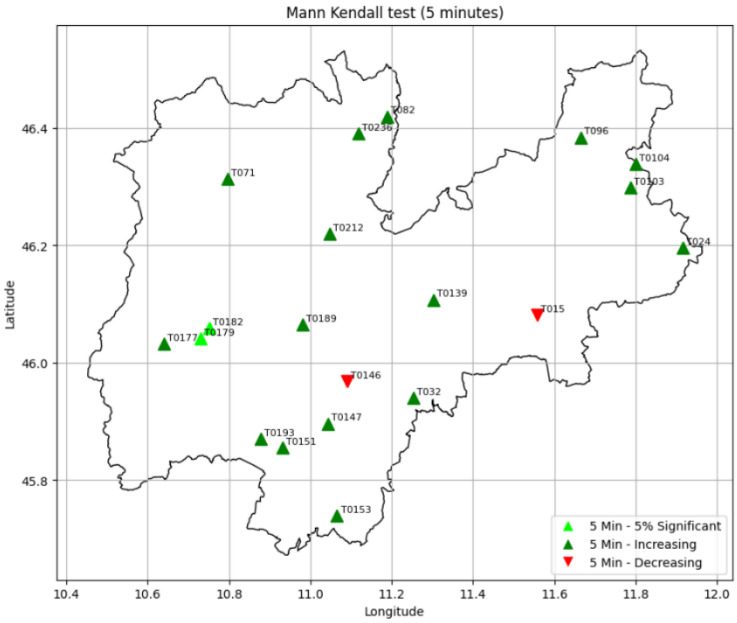

Figure 4.1: Map of direction of Mann Kendall test for 5 minutes time resolution

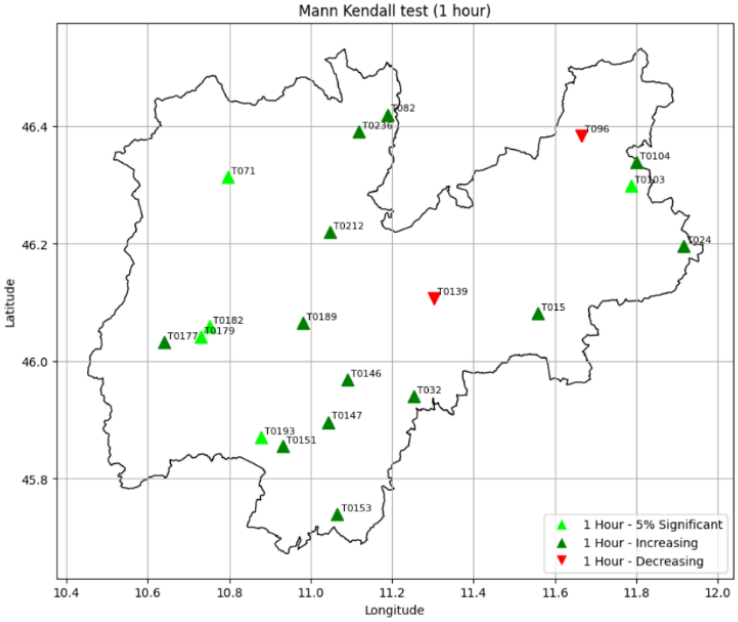

Figure 4.2: Map of direction of Mann Kendall test for 1 hour time resolution

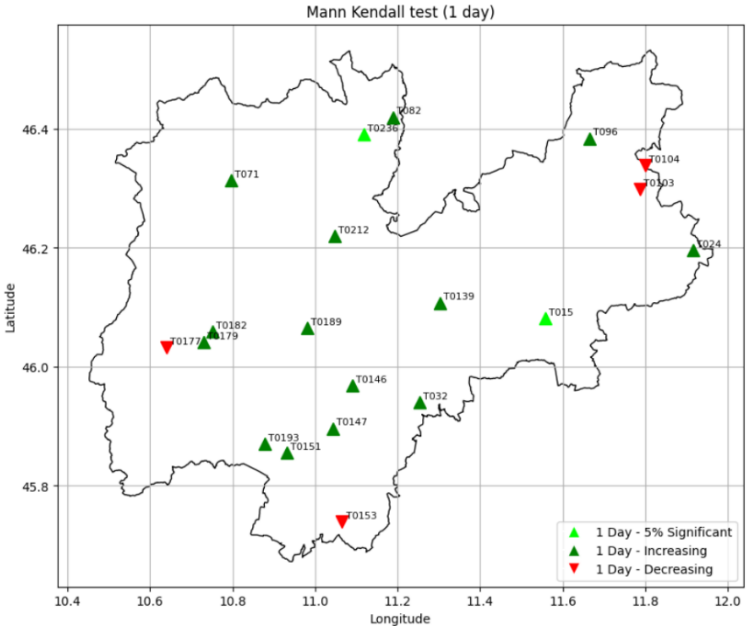

Figure 4.3: Map of direction of Mann Kendall test for 1 day time resolution

The maps presented depict regional trends in annual maximum rainfall across three distinct temporal resolutions: 5 minutes, 1 hour, and 1 day, analyzed using the non-parametric Mann-Kendall test. These trends suggest an overarching pattern of increasing intensity in rainfall extremes, signaling a notable shift in precipitation dynamics across the region.

Despite these observations, the statistical significance of these trends is largely limited, failing to meet the conventional 5% threshold. Notably, the analysis reveals that the 1-hour temporal resolution exhibits the most robust evidence of an upward trend in rainfall extremes. Conversely, as the temporal resolution increases to 1 day, there is an increase in the number of stations showing a negative trend, with four stations displaying a decline in extreme rainfall events.

To assess the magnitude of these observed trends and their implications for climate change, Theil-Sen slope estimators were utilized. These estimators were standardized by normalizing slopes relative to the duration in minutes, ensuring a consistent basis for comparison across different temporal scales. This normalization approach acknowledges the sensitivity of trend detection to the range and frequency of observations, thus facilitating a comprehensive evaluation of rainfall trends over varying time intervals.

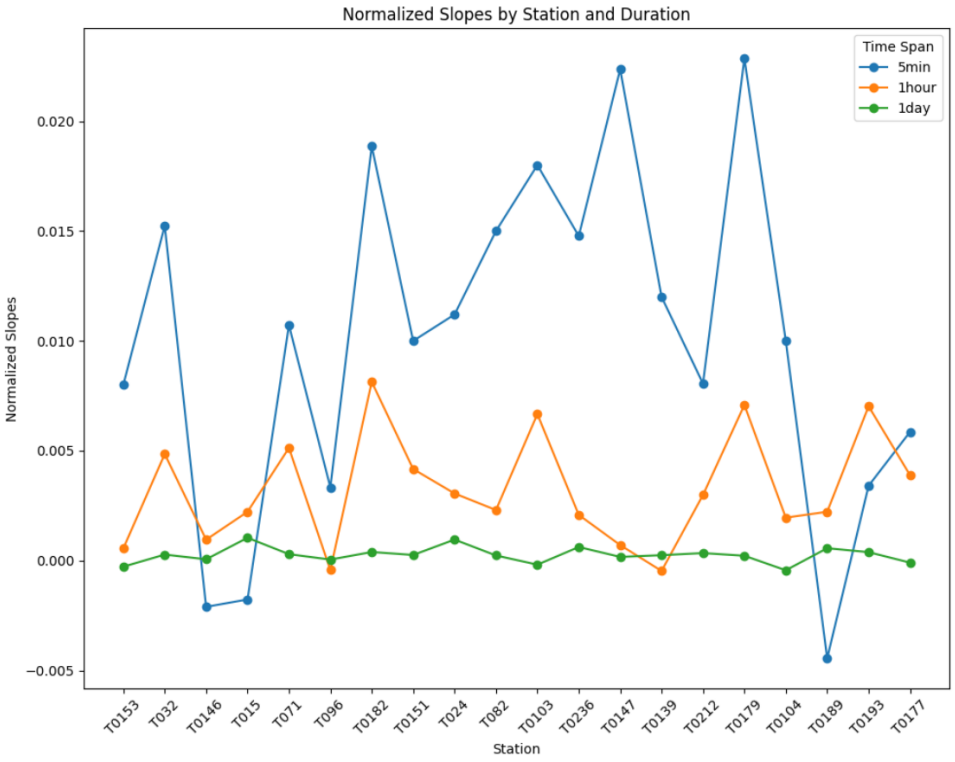

Figure 4.4: Normalized Sen Slopes across different Stations

The analysis of normalized Theil-Sen slope values reveals a significant trend towards increasing rainfall intensities for shorter durations (5 minutes) compared to longer durations (1 hour and 1 day), thereby supporting the hypothesis of intensified short-duration extreme events.

Specifically, a comprehensive examination of stations indicates that exactly 70% of them fully substantiate the original hypothesis. This finding implies that as rainfall duration decreases, there is a corresponding increase in the magnitude of intensity trends. This observation underscores a pronounced pattern where shorter rainfall durations exhibit more substantial changes in intensity.

In contrast, rainfall events observed at longer durations (1 day) demonstrate remarkable stability, with trends generally consistent across different stations. However, as the duration decreases, there is a notable exponential increase in variability among stations. This variability underscores the unpredictability of very extreme events, which exhibit diverse behavior even within a confined geographical area.

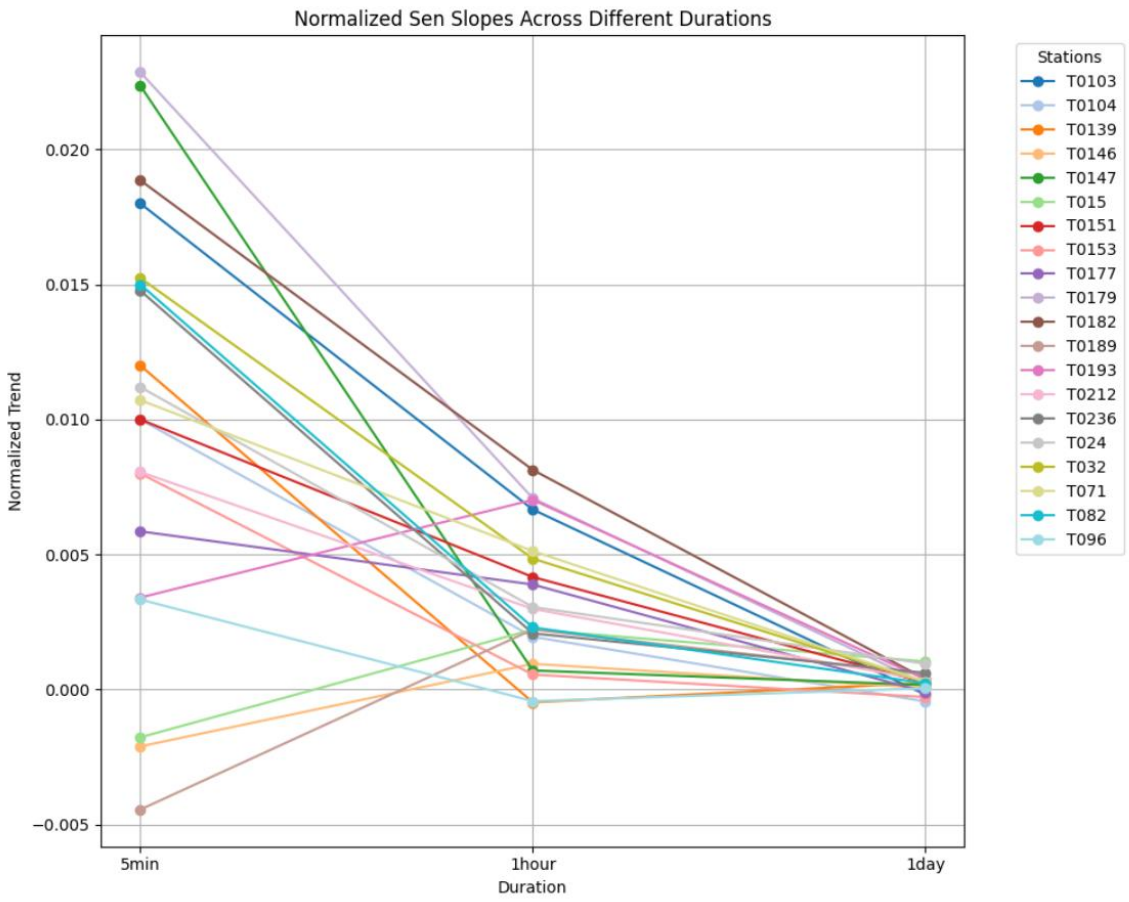

Figure 4.5: Normalized Sen Slopes across different Durations

The significant variability observed in shorter duration rainfall extremes provides compelling insights that challenge the initial hypothesis. This variability underscores the intricate nature of rainfall patterns, especially at finer time scales such as five minutes. While a majority of stations indicate intensified trends with decreasing duration, the wide range of observations at these shorter intervals suggests diverse and localized influences on precipitation dynamics. This variability calls for a nuanced interpretation of the data, recognizing that divergent observations can offer valuable insights into broader climate trends impacting the region.

To quantify the differences in average magnitude across durations, the average magnitude of each duration was calculated. Subsequently, the percentage change of the 1-hour and 1-day durations relative to the 5-minute time resolution was computed. This analysis aims to quantify how much the average magnitude of rainfall is increasing relative to one another.

The calculations reveal that the trend magnitude for the 5-minute duration is 3436.39% more intense than the slope observed for the 1-day duration, and 188.38% more intense compared to the 1-hour duration.

4.2 GEV MODELS

Among the several models explored, including stationary, linear time as a covariate, quadratic time as a covariate, linear temperature as a covariate, and quadratic temperature as a covariate, the decision to adopt the linear temperature model was informed by rigorous evaluation criteria such as the Akaike Information Criterion (AIC), the Bayesian Information Criterion (BIC), and log-likelihood values as well. These metrics collectively assessed the goodness of fit and model performance, revealing that the linear temperature model consistently demonstrated competitive performance across all evaluation criteria.

The stationary model consistently underperformed relative to the other models, confirming the non-stationarity of annual extreme rainfall, and the advantage in letting the location parameter to change, introducing covariates. The comparative analysis highlighted a particularly close performance between the linear temperature and quadratic time models. Despite their statistical similarity, the preference for the linear temperature model stemmed from several critical considerations. Firstly, the model's simplicity and interpretability were paramount. The linear relationship between temperature and extreme values offers a straightforward interpretation, where changes in temperature directly correlate with changes in the distribution of extreme events. In contrast, the quadratic time model introduces additional complexity without substantial empirical support in existing literature specific to the dataset.

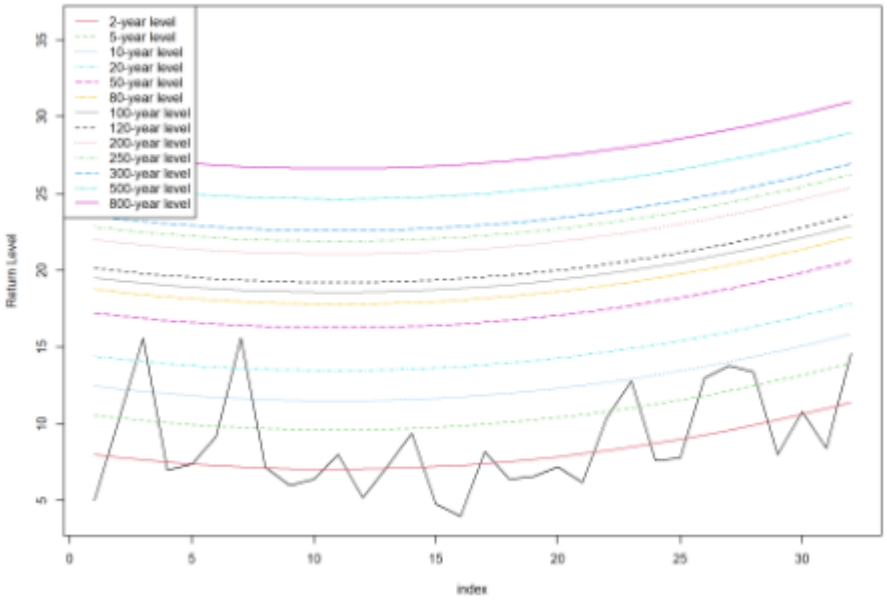

Figure 4.6: Return levels plot for the Quadratic Time covariate model (T0147)

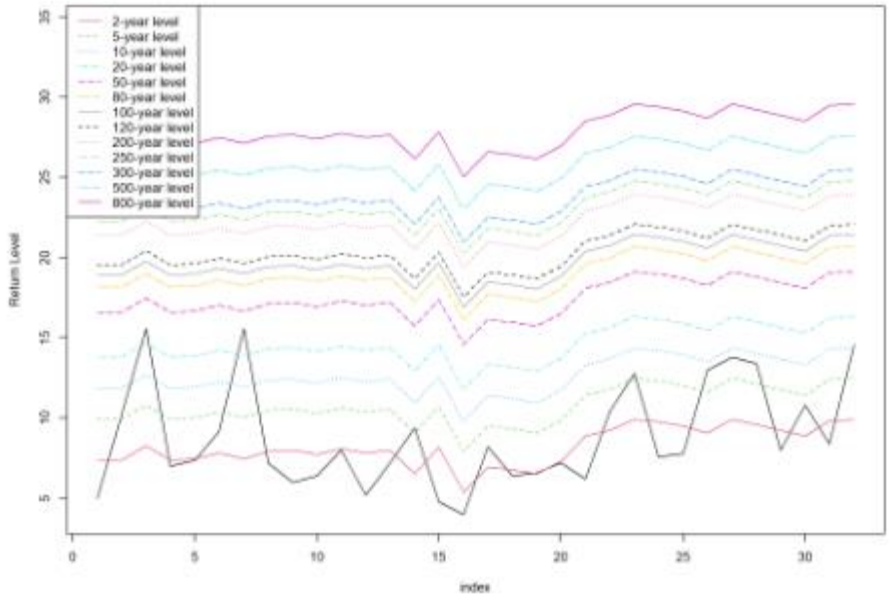

Figure 4.7: Return levels plot for the Linear Temperature covariate model (T0147)

It is fast forward, examining the return level plots for the fitted models for the Sample Station, how the temperature covariate predict better the behavior of the data, despite of the information criteria being extremely similar.

Moreover, opting for the linear temperature model aligns logically with climatological principles, where temperature plays a fundamental role in influencing weather extremes. This logical consistency not only enhances the model's interpretability but also underscores its practical utility in climate science and adaptation planning. Considering these factors, the dissertation emphasizes methodological rigor and theoretical coherence in selecting the linear temperature covariate within the GEV model.

5 CONCLUSION

5.1 DISCUSSION ABOUT THE RESULTS

The aim of this dissertation was to investigate changes in the distribution of extreme rainfall across the territory of Trentino, exploiting the detailed dataset provide. The study specifically focused on examining the intensification of short-duration and extremely short-duration (5 minutes) rainfall events compared to longer durations (1 day).

The results presented in Chapter 4 confirmed the hypotheses outlined in the introduction, revealing a significant increase in trends and their magnitude, particularly for short-duration rainfall events. However, it is noteworthy that only a few stations showed statistically significant trends at the 5% significance level. These findings are pivotal as they aligns with global climate change projections and emphasizes the sensitivity of extreme precipitation to temporal scales (Trenberth et al., 2015). The extreme high variability of shorter extreme rainfall extremes found in the data indicates the magnitude of local factor and characteristics, with a change in the distribution of rainfall. Some regions may experience more frequent and intense rainfall, while others may become drier. This shift in rainfall patterns can have significant impacts on water availability, agriculture, and ecosystems (Allen et al., 2010).

The non-stationarity of rainfall extremes has been investigated, with findings consistently confirming impact on extreme trend analysis. The performances of the models deployed in the thesis aligns with studies demonstrating that non-stationary Generalized Extreme Value models perform better stationary models in capturing precipitation patterns and trends (Huser et al., 2017; Heo and Kim, 2016). The findings underscore increasing temperatures as a phenomenon that highly contribute on the augmenting of extreme rainfall events, leading to increased evaporation and enhancing the atmosphere's moisture-holding capacity, relationship governed by the Clausius-Clapeyron equation (Allen & Ingram, 2002).

5.2 LIMITATION ON THE RESEARCH

Despite the valuable insights gained, several limitations need to be consideration in this study. The extreme variability observed in shorter duration trends underscores the necessity for a deeper understanding of these rainfall patterns. Factors such as topography, land use changes, and urbanization can both amplify and mitigate precipitation extremes, necessitating localized studies to accurately capture the diversity of the impacts.

Although the data utilized for the analysis provided valuable insights into evaluating precipitation behavior and patterns, the significant percentage of missing data over time has introduced bias about the reliability of the observations, making it challenging to perform accurate projections for the future. Furthermore, the study's constrained time span resulted in a relatively small sample size for conducting robust statistical analyses, narrowing the capability in capturing smaller, potentially meaningful effects and introducing uncertainty in estimation of the parameters and results.

5.3 SOCIO ECONOMIC AND FURTHER IMPLICATIONS

Extreme rainfall events are increasingly recognized for their profound socio-economic impacts, exerting significant pressures on communities, infrastructure, and economies worldwide. These events can lead to devastating consequences ranging from infrastructure damage to disruptions in economic activities and livelihoods. The economic repercussions of extreme precipitation events extend beyond immediate damage and losses. Long-term recovery and reconstruction efforts can strain public budgets and resources, diverting funds from other essential services such as healthcare and education (Ciscar et al., 2018). Governments and insurers face escalating costs associated with disaster response, compensation for damages, and investments in resilience measures (Kreibich et al., 2017).

This study underscores the critical role of continuous and updated high-quality data collection in improve the reliability of future projections, allowing precise risk assessment and to make informed climate adaptation policy decisions and resilience strategies.

5.4 CONCLUSION

The present dissertation investigated on the urgent phenomenon of the alteration of rainfall distribution, and the increase of extreme precipitation events, that have catastrophic impact on economic and society.

The findings aligned with several evidence from studies across the globe and underscored the urgency of proactive climate action, in order to develop adaptive strategies and resilient infrastructure. An effort is required in order to enhance high quality data collection in order to have the capability to perform precise statistical projections and have accuracy in projections.

6 REFERENCES

Aditya, F., et al. (2021). Rainfall trend analysis using Mann-Kendall and Sen's slope estimator test in West Kalimantan. IOP Conference Series: Earth and Environmental Science, 893, 012006. https://doi.org/10.1088/1755-1315/893/1/012006

Allen, M. R., & Ingram, W. J. (2002). Constraints on future changes in climate and the hydrologic cycle. Nature, 419(6903), 224-232. https://doi.org/10.1038/nature01092

Ban, N., et al. "Future increases in short-duration rainfall extremes with warming inferred from atmospheric dynamics." Nature Communications, vol. 6, 2015, article no. 6019. https://doi.org/10.1038/ncomms7019

Berg, P., et al. "Strong increase in convective precipitation in response to higher temperatures." Nature Geoscience, vol. 6, 2013, pp. 181-185. https://doi.org/10.1038/ngeo1731

Bogaard, T., et al. "Flood Damage Estimation for Swiss Alpine Regions: Data Sources, Uncertainties, and Model Evaluation." Natural Hazards and Earth System Sciences, vol. 20, no. 3, 2020, pp. 759-779. https://doi.org/10.5194/nhess-20-759-2020

Cai, Y., & Hames, D. (2010). Minimum sample size determination for generalized extreme value distribution. Communications in Statistics - Simulation and Computation, 40(01), 87-98. https://doi.org/10.1080/03610918.2010.530368

Ciscar, J. C., et al. (2018). "Climate Impacts in Europe: The JRC PESETA II Project." Journal of Extreme Events, 5(1), 1850005. https://doi.org/10.1142/S2345737618500053

Coles, S. (2001). An Introduction to Statistical Modeling of Extreme Values. Springer. https://doi.org/10.1007/978-1-4471-3675-0

Deloitte. (2022). Global turning point: The impact of climate change on the economy. Retrieved from https://www.deloitte.com/an/en/issues/climate/global-turning-point.html

De Paola, F., Giugni, M., Pugliese, F., Annis, A., & Nardi, F. (2018). GEV Parameter Estimation and Stationary vs. Non-Stationary Analysis of Extreme Rainfall in African Test Cities. Hydrology, 5(2), 28. https://doi.org/10.3390/hydrology5020028

Eurostat. (2022). Total economic loss caused by weather- and climate-related extreme events in EEA member countries (1980-2020). European Environment Agency. Retrieved from https://www.eea.europa.eu/publications/economic-loss-caused-by-weather

Ferreira, A., & de Haan, L. (2015). On the block maxima method in extreme value theory: PWM estimators. The Annals of Statistics, 43(1), 276–298. https://doi.org/10.1214/14-AOS1280

Fischer, E. M., & Knutti, R. (2016). Observed heavy precipitation increase confirms theory and early models. Nature Climate Change, 6(11), 986-991. https://doi.org/10.1038/nclimate3110

Gadedjisso-Tossou, A. G., Adjegan, K. I., & Kablan, A. K. M. (2021). Rainfall and Temperature Trend Analysis by Mann–Kendall Test and Significance for Rainfed Cereal Yields in Northern Togo. Sci, 3(1), 17. https://doi.org/10.3390/sci3010017

Heo, J. H., & Kim, T. W. (2016). "Nonstationary frequency analysis of extreme rainfall using the Generalized Extreme Value distribution." Water Resources Research, 52(1), 54-69. https://doi.org/10.1002/2015WR017065

Hinkel, J., et al. "Coastal Flood Damage and Adaptation Costs Under 21st Century Sea-Level Rise." Proceedings of the National Academy of Sciences, vol. 111, no. 9, 2014, pp. 3292-3297. https://doi.org/10.1073/pnas.1222469111

Huser, R., et al. (2017). "How much does non-stationarity affect the identification of precipitation trends?" Journal of Hydrology, 548, 601-612. https://doi.org/10.1016/j.jhydrol.2017.03.006

IPCC, 2021: Climate Change 2021: The Physical Science Basis. Contribution of Working Group I to the Sixth Assessment Report of the Intergovernmental Panel on Climate Change [Masson-Delmotte, V., P. Zhai, A. Pirani, S. L. Connors, C. Péan, S. Berger, N. Caud, Y. Chen, L. Goldfarb, M. I. Gomis, M. Huang, K. Leitzell, E. Lonnoy, J.B.R. Matthews, T. K. Maycock, T. Waterfield, O. Yelekçi, R. Yu and B. Zhou (eds.)]. Cambridge University Press. In Press.

Lenderink, G., Mok, H. Y., Lee, T. C., & van Oldenborgh, G. J. (2011). Super-Clausius–Clapeyron scaling of extreme hourly convective precipitation and its relation to large-scale atmospheric conditions. Journal of Climate, 24(11), 4753-4764. https://doi.org/10.1175/2011JCLI4097.1

Lenderink, G., et al. "Scaling potential and biases of climate model simulations of heavy precipitation events: A case study over France." Journal of Climate, vol. 30, 2017, pp. 3249-3267. https://doi.org/10.1175/JCLI-D-16-0477.1

Liu, Y., et al. "Driving Effects and Spatial-Temporal Variations in Economic Losses Due to Flood Disasters in China: Economic Loss Prediction of Flooding." Water, vol. 11, no. 10, 2019, article no. 2067. https://doi.org/10.3390/w11102067

Jayaweera, L., Wasko, C., Nathan, R., & Johnson, F. (2023). Non-stationarity in extreme rainfalls across Australia. Journal of Hydrology, 624, 129872. https://doi.org/10.1016/j.jhydrol.2023.129872

Kendon, E. J., et al. "Heavier summer downpours with climate change revealed by weather forecast resolution model." Nature Climate Change, vol. 4, 2014, pp. 570-576. https://doi.org/10.1038/nclimate2258

Kotz, S., & Nadarajah, S. (2000). Extreme Value Distributions: Theory and Applications. London: Imperial College Press. https://doi.org/10.1142/p191

Kreibich, H., et al. (2017). "Assessing economic resilience to flooding in cities—a social network analysis of impacts on residents." Environmental Science & Policy, 76, 38-47. https://doi.org/10.1016/j.envsci.2017.06.008

Marvel, K., Pendergrass, A. G., & Bonfils, C. J. (2019). Avoided warming of the Southern Ocean and South Pacific Ocean outweighs the enhanced greenhouse effect. Nature Climate Change, 9(9), 749-754. https://doi.org/10.1038/s41558-019-0557-8

Min, J. L. J., & Halim, S. A. (2020). Rainfall Modelling using Generalized Extreme Value Distribution with Cyclic Covariate. Mathematics and Statistics, 8(6), 762-772. https://doi.org/10.13189/ms.2020.080617

Nurse, L. A., et al. (2014). Small islands. In V. R. Barros, C. B. Field, D. J. Dokken, M. D. Mastrandrea, K. J. Mach, T. E. Bilir, ... & L. L. White (Eds.), Climate Change 2014: Impacts, Adaptation, and Vulnerability. Part B: Regional Aspects. Contribution of Working Group II to the Fifth Assessment Report of the Intergovernmental Panel on Climate Change (pp. 1613-1654). Cambridge University Press.

Peter, M., Rust, H. W., & Ulbrich, U. (2024). Interannual variations in the seasonal cycle of extreme precipitation in Germany and the response to climate change. Natural Hazards and Earth System Sciences, 24(4), 1261–1285. https://doi.org/10.5194/nhess-24-1261-2024

Pfahl, S., O'Gorman, P. A., & Fischer, E. M. (2017). Understanding the regional pattern of projected future changes in extreme precipitation. Nature Climate Change, 7, 423-427. https://doi.org/10.1038/nclimate3287

Prein, A. F., et al. "The future intensification of hourly precipitation extremes." Nature Climate Change, vol. 7, 2017, pp. 48-52. https://doi.org/10.1038/nclimate3168

Prein, A. F., Rasmussen, R. M., & Wehner, M. F. (2017). Challenges in 21st century climate simulations. Nature Climate Change, 7(10), 749-753. https://doi.org/10.1038/nclimate3398

Sen, P. K. (1968). Estimates of the regression coefficient based on Kendall's tau. Journal of the American Statistical Association, 63(324), 1379-1389. https://doi.org/10.1080/01621459.1968.10480934

Siddique, R., et al. "Quantifying Urban Flood Risk Under Climate Change: An Application of a Multihazard Framework to the Houston Metropolitan Region." Natural Hazards Review, vol. 21, no. 3, 2020, article no. 04020012. https://doi.org/10.1061/(ASCE)NH.1527-6996.0000365

Sudarsan, G., & A, L. (2023). Rainfall trend analysis using Mann-Kendall and Sen's slope test estimation- A case study. E3S Web of Conferences, 405, 04013. https://doi.org/10.1051/e3sconf/202340504013

Taguchi, R., et al. "Global-Scale Assessment of Economic Losses Caused by Flood-Related Business Interruption." Natural Hazards and Earth System Sciences, vol. 19, no. 9, 2019, pp. 2051-2072. https://doi.org/10.5194/nhess-19-2051-2019

Tran, H. Q., et al. "Assessing flood hazard using flood marks and analytic hierarchy process approach: a case study for the 2013 flood event in Quang Nam, Vietnam." Natural Hazards, February 2018, 90(1).

Trenberth, K. E., Fasullo, J. T., & Shepherd, T. G. (2015). Attribution of climate extreme events. Nature Climate Change, 5, 725-730. https://doi.org/10.1038/nclimate2657

United Nations Development Programme (UNDP). "Human Development Report 2020: The Next Frontier, Human Development and the Anthropocene." United Nations Development Programme, 2020.

Villarini, G., et al. "Recent trends in US flood risk." Nature Geoscience, vol. 14, 2021, pp. 1-7. https://doi.org/10.1038/s41561-020-00681-z

World Bank. "Future of Food: Shaping a Climate-Resilient Global Food System." World Bank Group, 2019. https://doi.org/10.1596/978-1-4648-1327-9

World Bank. (2024). Climate change and extreme poverty. World Bank.

Yin, Z., et al. "Assessing the Economic Impacts of Future Fluvial Flooding." Natural Hazards and Earth System Sciences, vol. 18, no. 2, 2018, pp. 365-387. https://doi.org/10.5194/nhess-18-365-2018

Yue, S., & Wang, C. (2004). The Mann-Kendall Test Modified by Effective Sample Size to Detect Trend in Serially Correlated Hydrological Series. Water Resources Management, 18(2004), 201–218. https://doi.org/10.1023/B:WARM.0000043140.61082.60

Zhang, X., & Villarini, G. (2020). Attribution of changes in rainfall and streamflow characteristics in a changing climate: a review. Wiley Interdisciplinary Reviews: Water, 7(1), e1406. https://doi.org/10.1002/wat2.1406